Annual Technical Report

Research Related to the Development, Fabrication and Characterization of UV Detectors and Cold Cathode Devices

R. F. Davis, A. D. Banks, E. Carlson, M. D. Bremser, A. D. Hanser,
P. Hartlieb, O.-H. Nam, W. G. Perry, C. Ronning, S. Smith,
R. Therrien, D. B. Thomson, and T. S. Zheleva
North Carolina State University
Materials Science and Engineering Department
Campus Box 7907
Raleigh, NC 27695

DTIC QUALITY INSPECTED 3

December, 1997

19980223 089

REPORT DOCUMENTATION PAGE

Public reporting burden for this collection of information is estimated to average 1 hour per response, including the time for reviewing instructions, searching existing data sources, gathering and maintaining the data needed, and completing and reviewing the collection of information. Send comments regarding this burden estimate or any other aspect of this collection of information, including suggestions for reducing this burden to Washington Headquarters Services, Directorate for Information Operations and Reports, 1215 Jefferson Davis Highway, Suite 1204, Arlington, VA 22202-4302, and to the Office of Management and Budget Paperwork Reduction Project (0704-0188), Washington, DC 20503.

1. AGENCY USE ONLY (Leave blank)	2. REPORT DATE	3. REPORT TYPE AND DATES COVERED
	December, 1997	Annual Technical 1/1/97-12/31/97

4. TITLE AND SUBTITLE

Research Related to the Development, Fabrication and Characterization of UV Detectors and Cold Cathode Devices

6. AUTHOR(S)

R. F. Davis

5. FUNDING NUMBERS

s400003srr14
1114SS
N00179
N66005
4B855

7. PERFORMING ORGANIZATION NAME(S) AND ADDRESS(ES)

North Carolina State University
Hillsborough Street
Raleigh, NC 27695

8. PERFORMING ORGANIZATION REPORT NUMBER

N00014-96-1-0765

9. SPONSORING/MONITORING AGENCY NAMES(S) AND ADDRESS(ES)

Sponsoring: ONR, Code 312, 800 N. Quincy, Arlington, VA 22217-5660
Monitoring: Admin. Contracting Officer, ONR, Regional Office Atlanta
101 Marietta Tower, Suite 2805
101 Marietta Street
Atlanta, GA 30323-0008

10. SPONSORING/MONITORING AGENCY REPORT NUMBER

11. SUPPLEMENTARY NOTES

12a. DISTRIBUTION/AVAILABILITY STATEMENT

Approved for Public Release; Distribution Unlimited

12b. DISTRIBUTION CODE

13. ABSTRACT (Maximum 200 words) Page 1 of 2

The microstructure and the mechanism of lateral epitaxy overgrowth (LEO) of homoepitaxially and selectively grown GaN pyramid structures on GaN/AlN/6H-SiC(0001) substrates and within windows in SiO_2 masks have been investigated by transmission electron microscopy (TEM) and scanning electron microscopy (SEM). The structures were produced by organometallic vapor phase epitaxy (OMVPE) for field emission studies. The SiO_2 film provided an amorphous stage on which lateral growth of the GaN occurred. Essentially no GaN deposited on the SiO_2 because of the substantial differences in sticking coefficients of Ga and N species on GaN (s=1) and SiO_2 (s~0). LEO of GaN layers has been achieved on 3 μm wide and 7 μm spaced stripe windows contained in SiO_2 masks. A high density of threading dislocations, originating from the interface of the underlying GaN with the AlN buffer layer, were contained in the GaN grown in the window regions. The overgrowth regions, by contrast, contained a very low density of dislocations. The second lateral epitaxial overgrowth layers were obtained on the first laterally grown layers by the repetition of SiO_2 deposition, lithography and lateral epitaxy. A GaN and $Al_xGa_{1-x}N$ thin film MODFET structure was grown for Northrup Grumman. The microstructures and photoluminescence spectra have been determined for $In_xGa_{1-x}N$ films (x ≤ ~0.23) grown on substrates of α(6H)-SiC(0001) wafer/AlN buffer layer/GaN heterostructures by low pressure OMVPE at 780°C using nitrogen as the diluent and carrier gas and V/III ratios as low as 2,420. Indium droplets were not observed. The InN content in these films was limited by the deposition pressure in the system. The maximum InN content achievable at 45 Torr was ~13%. Increasing the deposition pressure to 90 Torr increased the maximum InN content to ~23%. Room

14. SUBJECT TERMS

GaN, $Al_xGa_{1-x}N$, films, lateral epitaxy, SiO_2 masks, OMVPE, threading dislocations, pyramid, LEO, transmission electron microscopy, scanning electron microscopy, MODFET, Hall measurements, $In_xGa_{1-x}N$, indium droplets, InN, microstructure,

15. NUMBER OF PAGES

44

16. PRICE CODE

17. SECURITY CLASSIFICATION OF REPORT	18. SECURITY CLASSIFICATION OF THIS PAGE	19. SECURITY CLASSIFICATION OF ABSTRACT	20. LIMITATION OF ABSTRACT
UNCLAS	UNCLAS	UNCLAS	SAR

NSN 7540-01-280-5500

Standard Form 298 (Rev. 2-89)
Prescribed by ANSI Std Z39-18
298-102

REPORT DOCUMENTATION PAGE

1. AGENCY USE ONLY (Leave blank)	2. REPORT DATE	3. REPORT TYPE AND DATES COVERED
	December, 1997	Annual Technical 1/1/97-12/31/97

4. TITLE AND SUBTITLE

Research Related to the Development, Fabrication and Characterization of UV Detectors and Cold Cathode Devices

6. AUTHOR(S)

R. F. Davis

5. FUNDING NUMBERS

s400003srr14
1114SS
N00179
N66005
4B855

7. PERFORMING ORGANIZATION NAME(S) AND ADDRESS(ES)

North Carolina State University
Hillsborough Street
Raleigh, NC 27695

8. PERFORMING ORGANIZATION REPORT NUMBER

N00014-96-1-0765

9. SPONSORING/MONITORING AGENCY NAMES(S) AND ADDRESS(ES)

Sponsoring: ONR, Code 312, 800 N. Quincy, Arlington, VA 22217-5660
Monitoring: Admin. Contracting Officer, ONR, Regional Office Atlanta
101 Marietta Tower, Suite 2805
101 Marietta Street
Atlanta, GA 30323-0008

10. SPONSORING/MONITORING AGENCY REPORT NUMBER

11. SUPPLEMENTARY NOTES

12a. DISTRIBUTION/AVAILABILITY STATEMENT

Approved for Public Release; Distribution Unlimited

12b. DISTRIBUTION CODE

13. ABSTRACT (Maximum 200 words)   Page 2 of 2

temperature and 12 K PL spectra of the films revealed single-feature, near band edge (NBE) emission with increasing full width at half maximum (FWHM) values with increasing In fraction. The PL NBE FWHM for an $In_{0.23}Ga_{0.77}N$ film at 12 K was 103 meV. The electrical properties of Mg-doped GaN films grown via MOVPE have been characterized using capacitance voltage (C-V) and Hall measurements. The metallization scheme for the ohmic contacts which facilitated these measurements consisted of the deposition via electron beam evaporation of the double layer of 500Å Ni/1000Å Au. The as-deposited contacts were linear with a slight offset. Hall measurements showed carrier concentrations as high as 2×10^{17} cm^{-3} and a mobility of ~ 13.0 cm^{2}Volt^{-1} sec^{-1}. By comparison, the C-V data showed carrier concentrations from 3×10^{17}cm^{-3} to 5×10^{18}cm^{-3}. The etching behavior of gallium nitride, aluminum gallium nitride, and aluminum nitride has been systematically examined in an inductively coupled plasma (ICP) using Cl_2 and Ar as the reagents. Etch rates were strongly influenced by ICP power and DC bias. These rates were relatively insensitive to pressure, flow rate, and gas composition. Maximum etch rates of 9,800 Å/min for GaN, 9,060 Å/min for $Al_{.28}Ga_{.72}N$, and 7,490 Å/min for AlN were attained. The etch profiles were highly anisotropic over the range of conditions studied. The DC bias had to exceed certain voltages before significant etch rates were obtained. These values were <-20 V for GaN, -40 V for $Al_{.28}Ga_{.72}N$, and >-50 V for AlN. As such, increasing selectivity for GaN over $Al_{.28}Ga_{.72}N$ and AlN was achieved at DC biases below -40 V. At -20 V, the GaN etch rates were 38 times greater than AlN and a factor of 10 greater than $Al_{.28}Ga_{.72}N$. These results demonstrate the importance of ion bombardment in the etching of these materials. Cubic BN has been deposited via electron beam evaporation. Special cleaning procedures have eliminated the cracking and spalling.

14. SUBJECT TERMS

photoluminescence, emission, capacitance voltage, metallization, ohmic contacts, inductively coupled plasma, cubic boron nitride, electron beam evaporation

15. NUMBER OF PAGES

44

16. PRICE CODE

17. SECURITY CLASSIFICATION OF REPORT	18. SECURITY CLASSIFICATION OF THIS PAGE	19. SECURITY CLASSIFICATION OF ABSTRACT	20. LIMITATION OF ABSTRACT
UNCLAS	UNCLAS	UNCLAS	SAR

Table of Contents

I. Introduction

The numerous potential semiconductor applications of the wide band gap III–nitrides has prompted significant research regarding their growth and development. Gallium nitride (wurtzite structure), the most studied in this group, has a bandgap of ≈3.4 eV and forms continuous solid solutions with both AlN (6.2 eV) and InN (1.9 eV). As such, materials with engineered band gaps are feasible for optoelectronic devices tunable in wavelength from the visible to the deep UV. The relatively strong atomic bonding of these materials also points to their application for high-power and high-temperature microelectronic devices. Diodes emitting light from the yellow into the blue regions of the spectrum, blue emitting lasers, and several types of high-frequency and high-power devices have recently been fabricated from these materials.

Single crystal wafers of GaN are not commercially available. Sapphire(0001) is the most commonly used substrate, although its lattice parameter and coefficients of thermal expansion are significantly different from that of any III-nitride. The heteroepitaxial nucleation and growth of monocrystalline films of GaN on any substrate and AlN on sapphire are difficult at elevated (>900°C) temperatures. Therefore, at present, for successful organometallic vapor phase epitaxy (OMVPE) of GaN films on sapphire, the use of the initial deposition of an amorphous or polycrystalline buffer layer of AlN [1,2] or GaN [3,4] at low-temperatures (450°-600°C) is necessary to achieve both nucleation and relatively uniform coverage of the substrate surface. Subsequent deposition at higher temperatures and concomitant grain orientation competition has resulted in films of GaN(0001) and various nitrides alloys of improved quality and surface morphology relative to that achieved by growth directly on this substrate.

By contrast, we have observed that AlN and $Al_xGa_{1-x}N$ alloys containing even low (x ≥ 0.05) concentrations of AlN deposited on 6H-SiC(0001) substrates at high (≥1000°C) temperatures undergo two-dimensional nucleation and growth with resulting uniform surface coverage. In this research, the use of a 1000 Å, monocrystalline, high-temperature (1100°C) AlN buffer has resulted in GaN films void of oriented domain structures and associated low-angle grain boundaries [5,6]. Monocrystalline films of $Al_xGa_{1-x}N$ (0.05 ≤ x ≤ 0.70) of the same quality have also been achieved at 1100°C.

The investigations to 1975 regarding III-Nitrides in terms of thin films growth, characterization, properties and device development have been reviewed by Kesamanly [7] and Pankove and Bloom [8]. The considerable progress accomplished in these areas in the intervening years has been reviewed in Refs. [9–16]. Research in the authors' group at NCSU employs both MOCVD and GSMBE to grow GaN and $Al_xGa_{1-x}N$ films on α(6H)-SiC(0001)$_{Si}$ substrates. Only the investigations involving the former technique are described herein.

Selective growth of particular microstructures have been used extensively for the fabrication of semiconductor devices such as quantum well, wire and dot structures, as well as

field emitter structures. The selective growth of GaN and $Al_{0.1}Ga_{0.9}N$ linear windows and GaN hexagonal pyramid arrays on dot-patterned GaN/sapphire substrates have been reported [17,18]. The first field emission from an undoped GaN hexagonal pyramid array on a GaN/sapphire substrate has also been observed [18], and the enhancement of field emission performance was recently reported [20]. Thus far, all research regarding selective growth of GaN has used sapphire substrates. However, in the present research, 6H-SiC substrates have been employed with excellent results.

In this reporting period, research has been conducted in the following areas: (1) lateral epitaxy overgrowth (LEO) and transmission electron microscopy of homoepitaxially and selectively grown GaN pyramid and stripe structures on GaN/AlN/6H-SiC(0001) substrates and within windows in SiO_2 masks, (2) fabrication and electrical characterization of a GaN and $Al_xGa_{1-x}N$ thin film MODFET structure for Northrup Grumman, (3) growth, doping and characterization of $In_xGa_{1-x}N$ films on 6H-SiC substrates, (4) deposition and characterization of double layers of 500Å Ni/1000Å Au for ohmic contacts to p-type GaN, (5) the application of the inductively coupled etching technique to produce device microstructures in GaN and AlN, and (6) the growth and characterization of cubic boron nitride. The following sections are self-contained in that they provide an introduction, results, discussion of results, conclusions and references for a given topic.

References

1. M. A. Khan, J. N. Kuznia, D. T. Olson, and R. Kaplan, J. Appl. Phys. **73**, 3108 (1993).
2. H. Amano, I. Akasaki, K. Hiramatsu, N. Koide, and N. Sawaki, Thin Solid Films **163**, 415 (1988).
3. J. N. Kuznia, M. A. Khan, D. T. Olson, R. Kaplan and J. Freitas, J. Appl. Phys. **73**, 4700 (1993).
4. S. Nakamura, Jpn. J. Appl. Phys. **30**, L1705 (1991).
5. T. W. Weeks, Jr., M. D. Bremser, K. S. Ailey, E. P. Carlson, W. G. Perry, R. F. Davis, Appl. Phys. Lett. **67**, 401 (1995).
6. T. W. Weeks, Jr., M. D. Bremser, K. S. Ailey,W. G. Perry, E. P. Carlson, E. L. Piner, N. A. El-Masry, and R. F. Davis, J. Mat. Res. J. **11**, 1081 (1996).
7. F. P. Kesamanly, Sov. Phys. Semicond. **8**, 147 (1974).
8. J. I. Pankove and S. Bloom, RCA Rev. **36**, 163 (1975).
9. R. F. Davis, *et al.*, J. Mater. Sci. Eng. B **1**, 77 (1988).
10. S. Strite and H. Morkoc, J. Vac. Sci. Technol. B **10**, 1237 (1992).
11. J. I. Pankove, in *Diamond, Silicon Carbide and Related Wide Bandgap Semiconductor Materials*, edited by J. T. Glass, R. F. Messier, and N. Fujimori, (Mater. Res. Soc. Sym Proc. Vol. 116, Pittsburgh, PA, (1990), 515-524.
12. R. F. Davis, Proc. IEEE **79**, 702 (1991).
13. H. Morkoç, *et al.*, J. Appl. Phys. **76**, 1363 (1994).
14. J. H. Edgar, J. Mater. Res. **7**, 235 (1992).
15. M. Henin, J. Microelectron. **23**, 500 (1992).
16. H. Morkoç S. Strite, G. B. Gao, M. E. Lin, B. Sverdlov, B. and M. Burns, J. Appl Phys. **76**, 1363 (1994).
17. S. Kitamura, K. Hiramatsu and N. Sawaki, Jpn. J. Appl. Phys. **34**, 2284 (1995).

18. R. D. Underwood, D. Kapolnek, B. P. Keller, S.Keller, S. P. DenBaars and U. K. Mishra, Topical Workshop on Nitrides, Nagoya, Japan, September (1995).
19. T. Tanaka, K. Uchida, A. Watanabe and S. Minagawa, Appl. Phys. Lett. **68**, 976 (1996).

II. Microstructure and Lateral Epitaxy Formation Mechanism of Selectively Grown GaN Pyramids

A. Introduction

Group III nitrides are being extensively investigated for microelectronic and optoelectronic device applications due to their wide direct band gap and good thermal, chemical and mechanical stability. Two examples of the numerous published reviews and compilations of this research are given in Refs. [1] and [2]. The negative electron affinity of AlN [3] and the low positive electron affinity of GaN [4, 5] also make them promising candidate materials for field emitters [5]. The selective growth of GaN hexagonal pyramids on patterned GaN(0001) films on sapphire [4,6,7] and 6H-SiC(0001) substrates [5,8] have been reported. The microstructure and the lateral epitaxy formation mechanism of selectively grown GaN hexagonal pyramids are reported in the present study.

B. Experimental Procedure

Selective homoepitaxial growth of GaN pyramids has been achieved on circular patterned GaN/AlN/6H-SiC(0001) multilayered structures having a top SiO_2 layer containing circular windows with 5 μm and 10 μm diameter. The nitride films were grown in a cold wall, vertical, pancake type, RF inductively heated OMVPE system. The experimental growth parameters of the films are described elsewhere [9]. The thicknesses of the AlN buffer layer and the subsequently grown GaN layer were 1000 Å and 1.75 μm, respectively. The SiO_2 layers were deposited via RF sputtering or low pressure chemical vapor deposition. The parameters for the selective OMVPE growth of the GaN pyramids have also been reported previously [5,8]. In the present research the morphology, defect microstructure and formation mechanism of the pyramids have been investigated by SEM (JEOL 6400 FE) and TEM (TOPCON 002B, 200 kV). Cross-sectional samples for TEM have been prepared using standard procedures involving the sequence of grinding, polishing and ion-milling.

C. Results

Each of the pyramids has six $(1\bar{1}01)$ side facets as observed via SEM and shown in Fig. 1. The final size of the base of the GaN pyramids, as well as their height, depend on the window-to-mask area ratios. Reduction of this ratio leads to an increase in the average diagonal width under the same growth conditions [8].

Cross-sectional TEM from a pyramid array is shown in Fig. 2. This figure reveals that the pyramids grow with sharp closed tops and as single crystals, as revealed from the selected area diffraction pattern shown as an inset. Observations with TEM also reveal that the GaN pyramids extend laterally at dimensions larger than the radii of the windows. A low magnification TEM micrograph of a portion of one GaN pyramid in the $[11\bar{2}0]$ orientation is

shown in Fig. 3(a). Representative distributions of the dislocations within the pyramid and the underlying GaN film are clearly observed. The defects in the initial GaN film are threading segments of dislocations perpendicular or nearly perpendicular to the interface plane and short dislocation half loops near the GaN/AlN interface. It is important to note that the dislocations extend into each pyramid only above the window areas. Thus, the microstructure of each pyramid is characterized by two distinct regions, denoted A and B and shown pictorially in Fig. 3(a) and schematically in Fig. 3(b). Region A, located above the window area, and corresponding to the vertical growth, contains dislocations at a density comparable with that of the underlying GaN film within ~3 μm distance from the GaN/GaN homoepitaxial interface. Most of the extended dislocations propagate throughout the GaN film from the GaN/AlN and AlN/6H-SiC interfaces. The main cause of the generation of these defects is the mismatch in
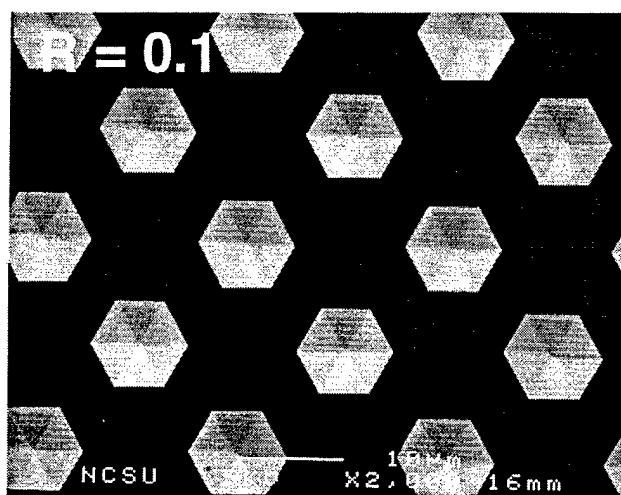

Figure 1.   SEM picture of a pyramid array grown at 0.1 ratio of the window-to-mask areas.
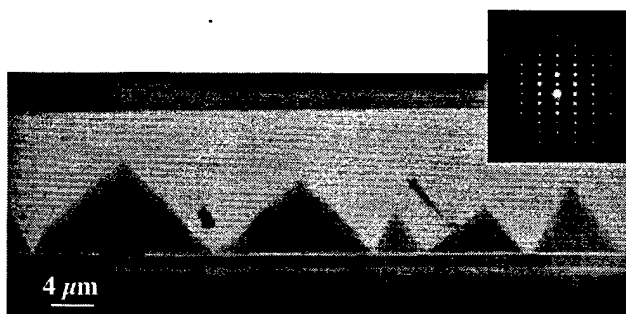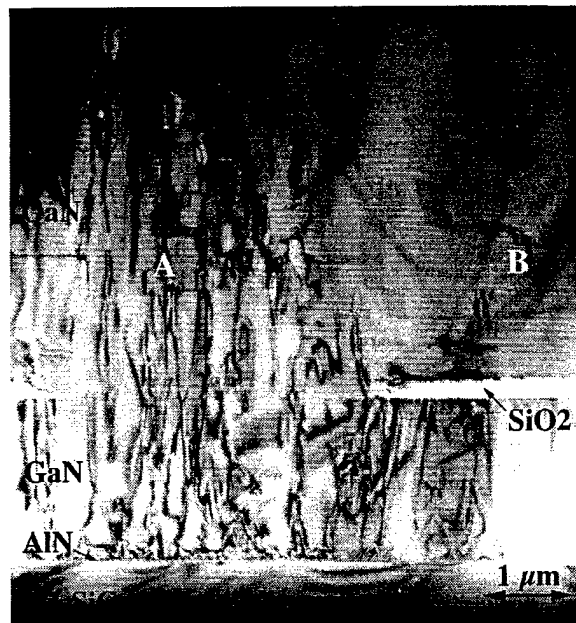

Figure 2.   Low magnification cross-sectional TEM of GaN pyramid array in [11$\bar{2}$0] orientation. The inset is a selected area diffraction pattern from a pyramid revealing its single crystal character.

5

(a)

(b)
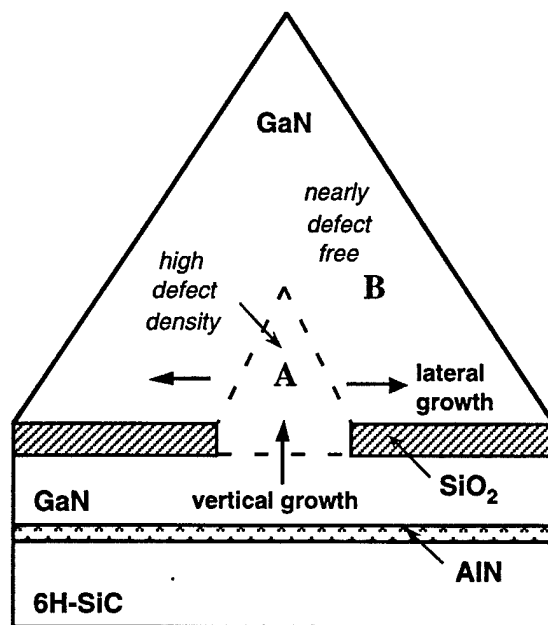
Figure 3.   (a) Microstructure of selectively grown GaN pyramid in $[11\bar{2}0]$ orientation of the foil. Two distinct regions are observed: region A located above the window in the SiO_2 and having a high dislocation density; and region B located above the mask with very few dislocations, with lines parallel to the interface plane and a low concentration of overlapping stacking faults (SF) close to the GaN/SiO_2 interface. (b) A schematic of the typical microstructure and lateral epitaxy mechanism of the selectively grown pyramid.

6

the lattice parameters at these interfaces. The final distribution of the dislocations is determined by the differences in both lattice parameters and coefficients of thermal expansion among these phases. The dislocation density diminishes within a pyramidal volume which ends at approximately one third of the pyramid height; no dislocations were observed at higher elevations in the pyramid structure.

Region B of the pyramid above the mask area surrounding the window, and corresponding to the lateral growth, is nearly free of observable defects. Very few short edge-on dislocation segments parallel to the interface plane and few overlapping stacking faults (SF) in the vicinity of the GaN pyramid/SiO_2 interface were observed. The high resolution TEM from the top and from the ($1\bar{1}01$) side walls of the pyramids again revealed material regions essentially free of dislocations, as shown in Fig. 4.

D. Discussion

The growth mechanism of the hexagonal pyramid structures in this study is lateral epitaxy. The two main stages of this mechanism are: (i) vertical growth and (ii) lateral growth [10]. During the first stage the deposited GaN grows selectively within the GaN windows more rapidly than it grows over the surrounding SiO_2 mask region due to the much higher sticking coefficient, s, of the Ga adatoms on the GaN surface (s=1) than on SiO_2 mask (s~0). This is the expected result as the SiO_2 bond strength is 799.6 kJ/mole and much higher than that of Si-N (439 kJ/mole), Ga-N (103 kJ/mole), and Ga-O (353.6 kJ/mole) [12]. Thus, it would be unlikely for Ga or N adatoms to bond to the SiO_2 surface in numbers and for a time sufficient to cause GaN nuclei to form. They would either evaporate or diffuse along the surface to the opening in the mask or to the vertical GaN surfaces which have emerged. During the second
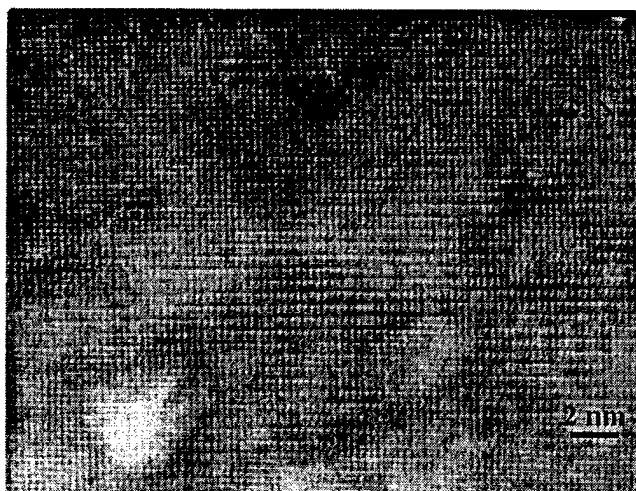

Figure 4.   High resolution TEM micrograph in [11$\bar{2}$0] orientation from the region close to the top of a GaN hexagonal pyramid revealing portions of areas of excellent lattice structure.

7

stage, the GaN grows simultaneously both vertically and laterally over the mask from the material which emerges over the windows. Surface diffusion of Ga and N on the SiO_2 may play a minor role in pyramid growth; however, the major source of material is derived from the gas phase. This has been demonstrated by the fact that an increase in the TEG flow rate causes the growth rate of the (0001) top facets to develop faster than the ($1\bar{1}01$) side facets and, thus, controls the lateral growth [7,8].

The laterally grown GaN is bonded to the underlying SiO_2 sufficiently strongly that it does not break away on cooling. However, lateral cracking within the SiO_2 is commonly but not universally observed in the samples as a result of thermal stresses generated on cooling. The nature of the bonding of the laterally grown GaN with the SiO_2, i.e., mechanical, chemical or both is not known at the time. The viscosity (ρ) of the SiO_2 at the growth temperature of 1050°C is $\sim 10^{15.5}$ poise which is one order of magnitude greater than the strain point ($\sim 10^{14.5}$ poise) where stress relief in bulk amorphous material occurs within approximately six hours [13].

Thus, the SiO_2 provides limited compliancy on cooling. As the atomic arrangement on the amorphous SiO_2 surface is quite different from that on the GaN surface, chemical bonding would occur only when appropriate pairs of atoms are in the close proximity. Extremely small relaxations of the Si and O and Ga and N atoms on the respective surfaces and/or within the bulk of the SiO_2 may accommodate the GaN and cause it to bond to the oxide.

Finally, the coalescence of the laterally growing volumes results in nearly defect free regions, as shown in Fig. 5. Detailed studies of the selective growth and the lateral epitaxy mechanism of the latter structures will be presented elsewhere.
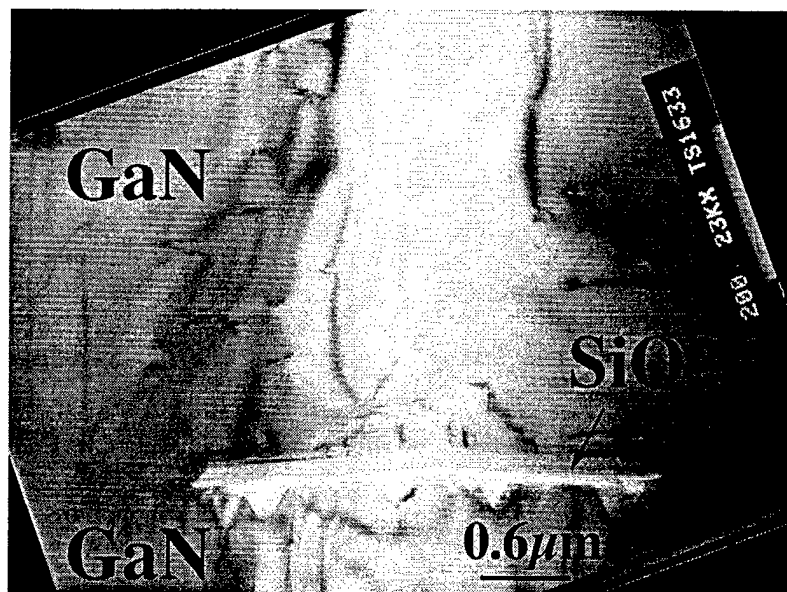

Figure 5.   Microstructure of a region of coalescence of two laterally grown areas of GaN in [$11\bar{2}0$] orientation of the foil.

E. Conclusions

In summary, single crystal hexagonal GaN pyramid arrays for field emission have been achieved via selective MOVPE growth on GaN/AlN/6H-SiC(0001) heterostructures within windows contained in the SiO_2 masks. Analysis with TEM revealed that lateral epitaxy over the SiO_2 provided the formation mechanism for large volume percentages of nearly defect free single crystal GaN. The TEG flow rate is a controlling factor in the lateral growth rate of the pyramids. Investigations regarding additional factors which control the growth rate and the optimization of the growth conditions are ongoing, as this process route has the potential as an alternative growth scheme to the conventional epitaxial growth of high quality GaN layered structures.

F. Acknowledgments

G. References

1. H. Morkoç, S. Strite, G. Gao, M. Lin, B. Sverdlov, and M. Burns, J. Appl. Physics **76** (3), 1363 (1994).
2. F.A. Ponce, T.D. Moustakas, I. Akasaki, B.A. Monemar, Ed., III-N Nitrides, MRS Symposium Proceedings **449**, 1997.
3. R. Nemanich, M. Bendjamin, S. Boseman, M. Bremser, S. King, B. Ward, R. F. Davis, B. Chen, Z. Zhang, and J. Bernholc, Materials Research Society Fall Meeting, Boston, November, 1995.
4. R. Underwood, D. Kapolnek, B. Keller, S. Keller, S. DenBaars, and U. Mishra, Topical Workshop on Nitrides, Nagoya, Japan, September (1995).
5. O. Nam, M. Bremser, B. Ward, R. Nemanich, and R. F. Davis, MRS Fall Meeting, Boston, November (1996).
6. Y. Kato, S. Kitamura, K. Hiramatsu, and N. Sawaki, J. Cryst. Growth **144**, 133 (1994).
7. S. Kitamura, K. Hiramatsu, and N. Sawaki, Jpn. J. Appl. Phys. **34**, 1184 (1985).
8. O. Nam, M. Bremser, B. Ward, R. Nemanich, and R. F. Davis, Jpn. J. Appl. Physics, 36, L532 (1997).
9. T. Warren Weeks, Jr., M. Bremser, K. Ailey, E. Carlson, W. Perry, E. Piner, N. El-Masry, R. F. Davis, J. Mater. Res. **11**, 1011 (1996).
10. E. I. Givargizov, *Oriented Crystallization on Amorphous Substrates*, Plenum Press, New York, 1991, pp. 221-264.
11. R. Underwood, D. Kapolnek, B. Keller, S. Keller, S. DenBaars, and U. Mishra, Submitted to Solid State Electronics.
12. D. Lide, Ed., *CRC Handbook of Chemistry and Physics*, 72nd ed., CRC Publishing, 1991-1992.
13. A. Varshneya, Fundamentals of Innorganic Glasses, Academic Press, New York, 1994, pp. 183-204.

III. Organometallic Vapor Phase Lateral Epitaxy of Low Defect Density GaN Layers

O. H. Nam, T. S. Zheleva, M. D. Bremser, D. B. Thomson, and R. F. Davis
Department of Materials Science and Engineering, North Carolina State University, Box 7907
Raleigh, NC 27695-7907

Abstract

Lateral epitaxial overgrowth (LEO) of GaN layers has been achieved on 3 m wide and 7 m spaced stripe windows contained in SiO_2 masks on GaN/AlN/6H-SiC(0001) substrates via organometallic vapor phase epitaxy (OMVPE). The extent and microstructural characteristics of lateral overgrowth were a complex function of stripe orientation, growth temperature and triethylgallium (TEG) flow rate. A high density of threading dislocations, originating from the interface of the underlying GaN with the AlN buffer layer, were contained in the GaN grown in the window regions. The overgrowth regions, by contrast, contained a very low density of dislocations. The second lateral epitaxial overgrowth layers were obtained on the first laterally grown layers by the repetition of SiO_2 deposition, lithography and lateral epitaxy.

A. Introduction

Conventional heteroepitaxial growth of GaN on low temperature GaN or AlN buffer layers previously deposited on Al_2O_3 and SiC substrates results in films containing high dislocation densities (10^8-10^{10} cm^{-2}) resulting from the mismatches in lattice parameters between the buffer layer and the film and/or the buffer layer and the substrate. This is believed to limit the performance of selected types of devices. Several groups [1-3] are investigating the growth of bulk GaN crystals from which would be derived substrates for growth of GaN and related films. However, at present, the size and growth rate of these crystals are limited.

The initial results of research regarding the lateral epitaxial overgrowth (LEO) of GaN layers on amorphous SiO_2 have been reported by the authors [4,5]. Additional results from studies [6] concerning the selective growth of GaN hexagonal pyramids for field emitters showed that lateral overgrowth unintentionally occurred over the SiO_2 mask layers under selected growth conditions. Transmission electron microscopic study also revealed that these overgrown regions of pyramids contained a very low density of dislocation ($<10^4$ cm^{-2}) [7].

Following the reports of our research [4,5], Nakamura [8] reported a substantially increased laser diode life time of approximately 10,000 hours at room temperature in devices fabricated using the LEO technique. As a result, the LEO technique has received considerable interest from the III-Nitride research community.

The first lateral epitaxial overgrowth and coalescence of GaN stripes patterned in SiO_2 masks deposited on GaN film/AlN buffer layer/6H-SiC(0001) substrate assemblies and the second lateral epitaxial overgrowth on the first laterally overgrown GaN layer have more recently been accomplished and are described in the following sections.

B. Experimental Procedures

Substrates for the lateral epitaxy studies were prepared, as shown schematically in Fig. 1, via growth of 1.5-2.0 μm thick GaN films at 1000°C on high temperature (1100°C) AlN buffer layers previously deposited on 6H-SiC(0001) substrates in a cold-wall, vertical and RF inductively heated organometallic vapor phase epitaxy (OMVPE) system. Additional details of the growth experiments are given in Ref. 9. An SiO_2 mask layer (thickness = 1000 Å) was subsequently deposited on each GaN/AlN/6H-SiC(0001) sample via low pressure chemical vapor deposition at 410°C. Patterning of the mask layer was achieved using standard photolithography techniques. Etching was accomplished with a buffered HF solution. The pattern contained 3 m wide, parallel stripe openings spaced 7 μm from edge-to-edge and oriented along the <11$\bar{2}$0> and <1$\bar{1}$00> directions in each GaN film. Prior to lateral overgrowth, the patterned samples were dipped in a 50% buffered HCl solution to clean the underlying GaN layer.

The lateral overgrowth of GaN was achieved at 1000–1100°C and 45 Torr. Triethylgallium (13–39 μmol/min) and NH_3 (1500 sccm) precursors were used in combination with a 3000 sccm H_2 diluent. The second lateral epitaxial overgrowth was conducted on the first laterally grown layer via the repetition of SiO_2 deposition, lithography and lateral epitaxy, as shown in Fig. 1. The samples were characterized using scanning electron microscopy
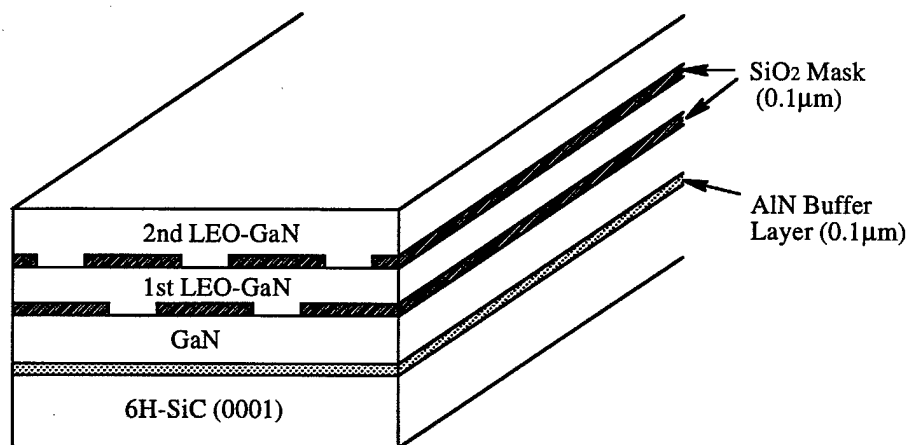

Figure 1.   Schematic diagram showing the first and second lateral epitaxial overgrowths of GaN layers from within stripe openings and over the top surfaces of two SiO_2 masks.

11

(SEM-JEOL 6400 FE), atomic force microscopy (AFM-Digital Instrument NanoScope III) and transmission electron microscopy (TEM-TOPCON 002B, 200KV).

C. Results and Discussion

Figure 2 shows the representative cross-sectional morphologies of two GaN stripes selectively grown for 60 min along <11$\bar{2}$0> and <1$\bar{1}$00>. Truncated triangular stripes having (1$\bar{1}$01) slant facets and a narrow (0001) top facet were observed for window openings along <11$\bar{2}$0>. Rectangular stripes having a (0001) top facet, (11$\bar{2}$0) vertical side facets and (1$\bar{1}$01) slant facets developed in samples grown along <1$\bar{1}$00>. Observations via SEM of GaN stripes grown for different times up to 3 min revealed similar morphologies regardless of stripe orientation. The stripes subsequently developed into different shapes if the growth was continued. The amount of lateral growth exhibited a strong dependence on stripe orientation. Results obtained under various growth conditions showed that the lateral growth rate of the <1$\bar{1}$00> oriented stripes was much faster than those along <11$\bar{2}$0>. We believe that the different morphological development as a function of window orientation is related to the stability of the crystallographic planes in the GaN structure. Stripes oriented along <11$\bar{2}$0> always had wide (1$\bar{1}$01) slant facets and either a very narrow or no (0001) top facet depending on the growth conditions. The primary reason for this is that (1$\bar{1}$01) is the most stable plane in the GaN wurtzite crystal structure, and the growth rate of this plane is lower than that of others. As shown in Fig. 2 (b), the {1$\bar{1}$01} planes of the <1$\bar{1}$00> oriented stripes were wavy, which implies the existence of more than one Miller index. It is believed that competitive growth of selected {1$\bar{1}$01} planes occurs during the deposition which causes these planes to become unstable and which causes their growth rate to increase relative to that of the (1$\bar{1}$01) plane of stripes oriented along <11$\bar{2}$0> [4].

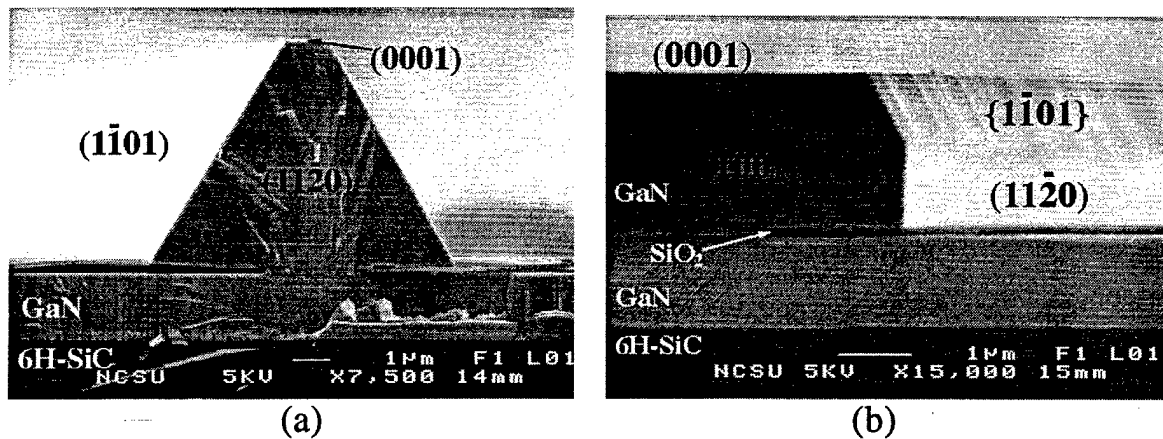(a)   (b)

Figure 2.   Scanning electron micrographs showing the morphologies of GaN layers grown on stripe openings oriented along (a) <11$\bar{2}$0> and (b) <1$\bar{1}$00>.

The morphological development of the GaN stripes also depends on the flow rate of the TEG, as shown in Fig. 3. An increase in the supply of TEG increased the growth rate of the stripes in both the lateral and the vertical directions. However, the lateral/vertical growth rate ratio decreased from 1.7 at the TEG flow rate of 13 mol/min to 0.86 at 39 mol/min. This increased influence on growth rate along <0001> relative to that of <11$\bar{2}$0> with TEG flow rate is believed to be related to the type of reactor employed in this research, wherein the reactant gases flow vertically and perpendicular to the substrate. The considerable increase in the concentration of the Ga species on the surface may sufficiently impede their diffusion to the {1$\bar{1}$01} planes such that chemisorption and GaN growth occur more readily on the (0001) plane. The morphologies of the GaN layers were also a strong function of the growth temperatures [4]. Stripes grown at 1000°C possessed a truncated triangular shape. This morphology gradually changed to the rectangular cross-section as the growth temperature was increased.

The first lateral epitaxial overgrown GaN layers with thickness of 2m were obtained using 3 m wide stripe openings spaced 7 m apart and oriented along <1$\bar{1}$00>, see Fig. 4(a). The growth parameters were 1100°C and a TEG flow rate of 26 mol/min. A plan view of the first lateral epitaxy layer revealed a microscopically flat and pit-free surface, see Fig. 4(b). Atomic force microscopy showed the surfaces of the laterally grown GaN layers to consist of a terrace structure having an average step height of 0.32 nm. The average RMS roughness values of the regrown and overgrown areas were 0.23 nm and 0.29 nm, respectively; these are similar to the values obtained for the underlying GaN films.

The second lateral epitaxial overgrowth of GaN layers on the first lateral epitaxy layers has also been achieved as shown in Fig, 4(c). This achievement was made through the repetition of SiO$_2$ deposition, lithography and lateral epitaxy. Each black spot in the overgrown GaN layers shown in Fig, 4(a) and 4(c) is a subsurface void which forms when two growth
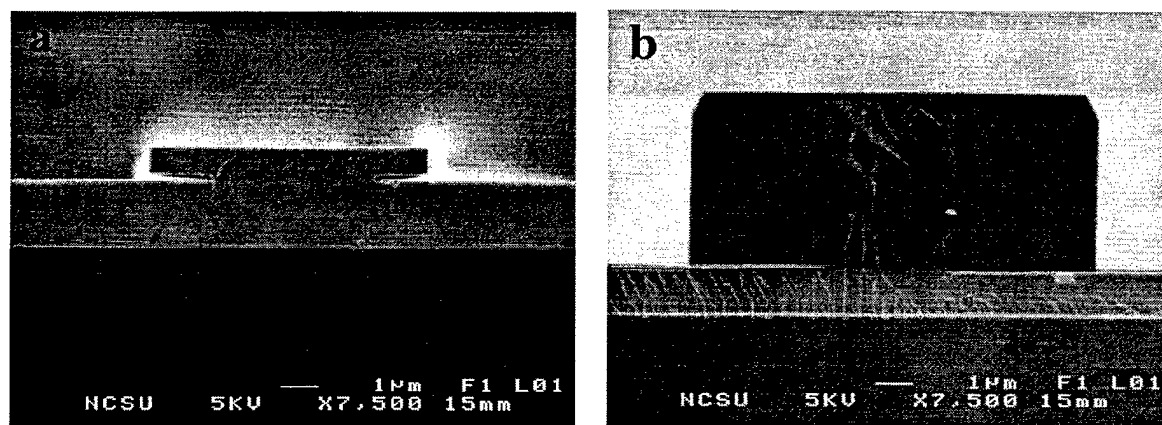

Figure 3. Scanning electron micrographs of <1$\bar{1}$00> oriented GaN stripes grown at TEG flow rates of (a) 13 mol/min and (b) 39 mol/min for 60min.

fronts coalesce. These voids were most often observed using the lateral growth conditions wherein rectangular stripes having vertical $\{11\bar{2}0\}$ side facets developed [5]. Surface morphology of the second overgrown layer was comparable to the first layer, as shown in Figure 4(d). Cracks were occasionally observed along the coalesced interface under selected growth conditions, probably due to the thermal mismatch between the GaN layers and the SiO_2 mask.

The micrograph obtained via cross-sectional TEM and presented in Fig. 5 shows a typical laterally overgrown GaN. Threading dislocations, originating from the GaN/AlN buffer layer interface, propagate to the top surface of the regrown GaN layer within the window regions of the mask. The dislocation density within these regions, calculated from the plan view TEM micrograph is approximately 10^9 cm^{-2}. By contrast, there were no observable threading dislocations in the overgrown layer [7]. Additional microstructural studies of the areas of lateral growth obtained using various growth conditions have shown that the overgrown GaN layers contain only a few dislocations. These dislocations formed parallel to the (0001) plane via the extension of the vertical threading dislocations after a 90° bend in the regrown region [7]. Plan view TEM observation revealed that these dislocations never propagate to the top surface of the overgrown GaN layers.

Cross-sectional TEM observation of the second LEO sample in the micrograph presented in Fig. 6 shows that a very low density of dislocations parallel to the (0001) plane, formed via bending of threading dislocation, exist in the first and second LEO-GaN layers on the SiO_2
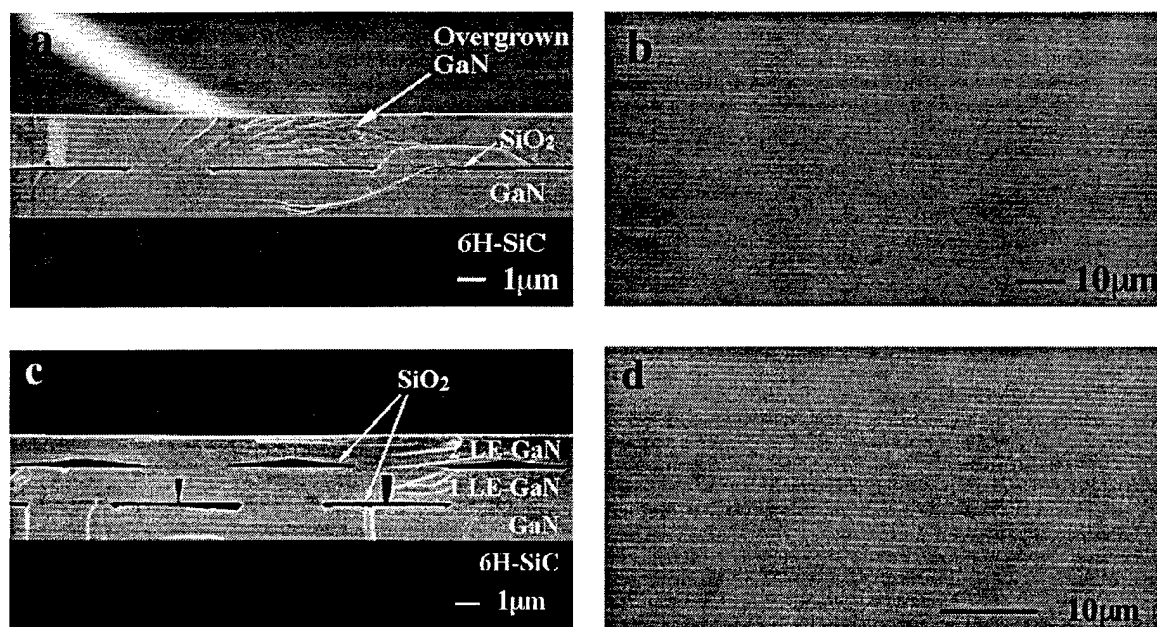

Figure 4.   Cross-section and surface SEM micrographs of the first, (a) and (b), and second, (c) and (d), coalesced GaN layers, respectively, grown on 3 m wide and 7 m spaced stripe openings oriented along <1$\bar{1}$00>.

14

masks. The second SiO$_2$ mask is slightly misaligned relative to the first. These results suggest that very low defect density GaN layers can be fabricated by precise alignment of the mask in the second lithographic process.

Preliminary photoluminescence and cathodoluminescence results indicated that yellow emission (2.25 eV) originates from the regrown regions having high dislocation densities; but only strong band edge emission has been observed from the overgrown layers. Donor-acceptor pair emission was also observed from the lateral overgrown layers. Studies including photoluminescence, cathodoluminescence and micro-Raman scattering are underway to determine correlations between the optical and the microstructural characteristics of the laterally overgrown GaN layers.
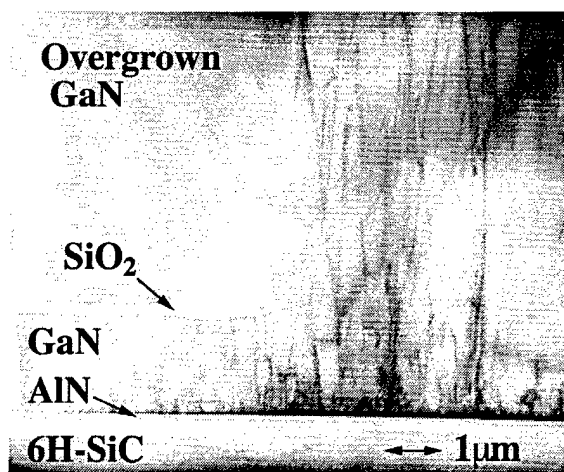

Figure 5.   Cross-section TEM micrograph of a section of a laterally overgrown GaN layer on an SiO$_2$ mask region.
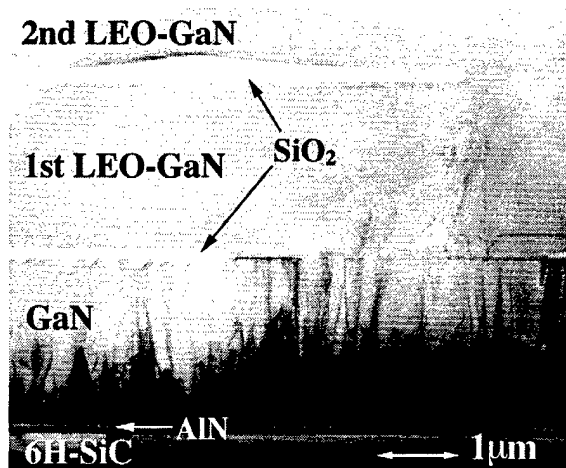

Figure 6.   Cross-section TEM micrograph of a section of the second lateral epitaxial overgrown GaN layers.

15

D. Conclusions

Lateral epitaxial overgrowth of GaN on SiO_2 masks containing stripe windows oriented along different orientations has been achieved via OMVPE. The morphological development of these stripes depended strongly on the stripe orientation and growth conditions. The first and second lateral epitaxy GaN layers with both extremely low densities of dislocations and smooth and pit-free surfaces has been obtained for the first time along <1$\bar{1}$00> at 1100C and a TEG flow rate of 26 mol/min.

E. Acknowledgments

F. References

1. S. Porowski, M. Bockowski, B. Lucznik, M. Wroblewski, S Krukowski, I Grzegory, M. Leszczynski, G. Nowak, K. Pakula and J. Baranowski, Mat. Res. Soc. Symp. Proc. **449**, 35 (1996).
2. S. Kurai, Y. Naoi, T. Abe, S. Ohmi and S. Sakai, Jpn. J. Appl. Phys. **35**, L77 (1996).
3. C.M. Balkas, Z. Sitar, T. Zheleva, L. Bergmann, I.K. Shmagin, J.F. Muth, R. Kolbas, R J. Nemanich and R.F. Davis, Mat. Res. Soc. Symp. Proc. **449**, 41 (1996).
4. O.H. Nam, M.D. Bremser, T.S. Zheleva and R.F. Davis, The 39th Electronic Materials Conference, Fort Collins, Colorado, June 25-27 (1997).
5. O.H. Nam, M.D. Bremser, T.S. Zheleva and R.F. Davis, Appl. Phys. Lett. **71**, 2638, (1997).
6. O.H. Nam, M.D. Bremser, B.L. Ward, R.J. Nemanich and R.F. Davis, Jpn. J. Appl. Phys. **36**, L532 (1997).
7. T.S. Zheleva, O.H. Nam, M.D. Bremser and R.F. Davis, Appl. Phys. Lett. **71**, 2472 (1997).
8. S. Nakamura, The 2nd Int. Conf. Nitride Semiconductors, Tokushima, Japan, October 25-31, (1997)
9. T.W. Weeks Jr., M.D. Bremser, K.S. Ailey, E.P. Calson, W.G. Perry and R.F. Davis, Appl. Phys. Lett. **67**, 401 (1995).

IV. Growth and Photoluminescence Properties of $In_xGa_{1-x}N$ Films Grown on SiC Substrates by Low Pressure Metalorganic Vapor Phase Epitaxy

A. D. Hanser, W. G. Perry, R. F. Davis
Department of Materials Science and Engineering, North Carolina State University
Raleigh, NC 27613-7907

Abstract

The microstructures and photoluminescence (PL) spectra have been determined for $In_xGa_{1-x}N$ films (x ≤ ~0.23) grown on substrates of α(6H)-SiC(0001) wafer/AlN buffer layer/GaN heterostructures by low pressure metalorganic vapor phase epitaxy at 780°C using nitrogen as the diluent and carrier gas and V/III ratios as low as 2,420. Indium droplets were not observed. The InN content in these films was limited by the deposition pressure in the system. The maximum InN content achievable at 45 Torr was ~13%. Increasing the deposition pressure to 90 Torr increased the maximum InN content to ~23%. Room temperature and 12 K PL spectra of the films revealed single-feature, near band edge (NBE) emission with increasing full width at half maximum (FWHM) values with increasing In fraction. The PL NBE FWHM for an $In_{0.23}Ga_{0.77}N$ film at 12 K was 103 meV.

A. Introduction

Gallium nitride (GaN) and the related alloys $In_xGa_{1-x}N$ and $Al_xGa_{1-x}N$ are the current materials of choice for the fabrication of light emitting diodes in the blue and green regions of the visible spectrum [1] and laser diodes in the blue and violet regions [2]. In these devices, $In_xGa_{1-x}N$ is the active layer and the wavelength of the emitted light is controlled by the InN content in the film. The weak In-N bond at the surface and the resultant high equilibrium vapor pressure of nitrogen [3,4] as well as the tendency to phase separate [5] are the main difficulties in growing In-containing materials. Films of $In_xGa_{1-x}N$ with relatively high InN content (> 10%) and without In droplets have recently been obtained by using high In source flow rates, high V/III ratios and lower growth temperatures [6-8]. The use of N_2 as the carrier and diluent gas instead of H_2 has also been shown to increase the InN incorporation in the films [9,10]. Metalorganic vapor phase epitaxy (MOVPE) at one atmosphere of pressure has been the primary method of growth for the $In_xGa_{1-x}N$ materials. Relatively little research using this technique for growth of these materials at reduced pressure has been conducted [11,12]. In this letter, the growth and photoluminescence (PL) properties of $In_xGa_{1-x}N$ films grown by low pressure MOVPE are reported.

B. Experimental Procedures

All films were grown on on-axis $\alpha(6H)$-SiC(0001) substrates using a MOVPE reactor described elsewhere [13]. A high temperature (1100°C) AlN film approximately 1000Å thick was grown directly on the substrate as a buffer layer. A 1 µm thick GaN film was then deposited as a template for the $In_xGa_{1-x}N$ films. The latter films were grown for 30 minutes at 780°C using trimethylindium (TMI) and triethylgallium (TEG) as the In and Ga sources, respectively. The TEG flow rate was 3.8 µmol/min and the TMI flow rate was varied between 5 and 30 µmol/min. N_2 was used as the carrier and diluent gas. The NH_3 flow rate was 0.082 mol/min (2 standard liters per minute). The growth experiments were conducted at 45 and 90 Torr. The films were characterized via scanning electron microscopy (SEM) using a JEOL 6400 FE microscope operating at 5 keV. Room temperature and low temperature (12 K) photoluminescence (PL) measurements were made using a 15 mW He-Cd laser (λ=325 nm) as the excitation source. All film compositions were determined from PL peak positions and compared to published compositional values.

C. Results and Discussion

The growth rate of the $In_xGa_{1-x}N$ films was approximately 2000Å/hr as measured by cross-sectional SEM. The surfaces of films with an InN content < ~10% were smooth with only a few pits for film thicknesses up to 1000Å, the largest thickness observed in this research. As the InN content increased over ~10% and the thicknesses of these films increased to over several hundred angstroms, a pitted and grooved morphology was observed, as shown

in Fig. 1. This surface morphology could be attributed to either strain in the film or a change in the growth mode for higher InN content films. The lattice parameter difference between GaN and InN (Δ/a_0) is 11.2% [14]. Assuming no phase separation, as the InN content of the $In_xGa_{1-x}N$ film increases the strain in the film increases due to increasing lattice mismatch between it and the underlying GaN layer. This increase in strain can lead to a change in the growth mode from two-dimensional (Frank-van der Merve) to three-dimensional growth (Stranski-Krastanov). With this latter growth mode, the coalescence of islands leads to layer formation and can result in the observed pitted and grooved surface morphology.

Under no growth conditions were In droplets observed. Previous research [8,15] has indicated the necessity of using V/III ratios in the range of 5,200–10,000 to eliminate the presence of In droplets; however, $In_xGa_{1-x}N$ films with approximately 23% InN content were grown in this research with a V/III ratio of approximately 2,420.

The InN content of the films was a function of reactor pressure during growth. Figure 2 shows the near band edge (NBE) emission peak positions at 12 K for $In_xGa_{1-x}N$ films grown under varying TMI flow rates as a function of reactor pressure. At 45 Torr the In incorporation in the film increased linearly with increasing TMI flow rate from 5 to 15 μmol/min. However, from 20 to 30 μmol/min the InN content remained constant at approximately 13%. At a reactor pressure of 90 Torr, the $In_xGa_{1-x}N$ NBE emission increases linearly with increasing TMI flow rate up to 30 μmol/min. This difference in In incorporation is due to the higher overpressure of gas at the growth surface at 90 Torr which reduces the ability of the In to desorb from
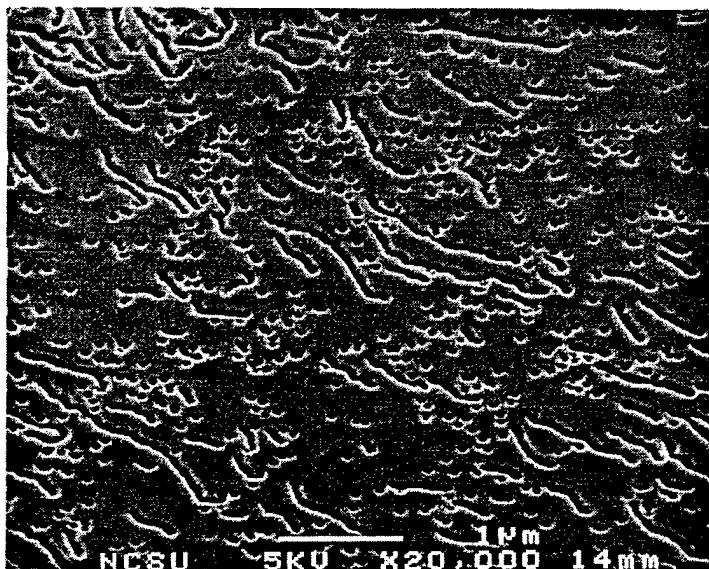

Figure 1.   SEM micrograph of the surface of an 1000Å $In_{0.23}Ga_{0.77}N$ film.

the surface. The rate of desorption of the source species from the growth surface during MOVPE growth is a kinetic process which can be represented by Eq. 1:

$$r_d = k_d \times n_d \qquad (1)$$

where r_d is the rate of desorption, k_d is the rate constant, and n_d is the number of atoms of evaporating species per unit area. The rate constant k_d is the fraction of these atoms evaporating per unit time and is a function of the temperature and pressure of the system. As the pressure is increased at a constant temperature, k_d will decrease and the number of atoms desorbing from the surface will be reduced. The larger number of gas phase collisions at the $In_xGa_{1-x}N$ growth surface due to the increased system pressure at 90 Torr decreases the number of In atoms desorbing from the surface, thus allowing more of this species to be incorporated during growth.

Figure 3 shows the 12 K PL of GaN and $In_xGa_{1-x}N$ films as a function of x from approximately 0.05 to 0.23. The peak intensities for all the films were on the same order of intensity. The compositions of the $In_xGa_{1-x}N$ films were determined using a least squares linear fit to data points from twelve published papers quoting $In_xGa_{1-x}N$ compositional values. The FWHM of the band edge related peaks increased with increasing In fraction, possibly due to an increase in the number of free carriers [12] or an increase in local variations of the film composition. The FWHM of the NBE peak for the PL spectra corresponding to an $In_{0.05}Ga_{0.95}N$ film centered at 372.4 nm (3.330 eV) was 52 meV; the analogous value for an $In_{0.23}Ga_{0.77}N$ film centered at 428.9 nm (2.891 eV) was 103 meV. The FWHM of the reference GaN NBE peak was 6.90 meV. No donor-to-acceptor pair (DAP) recombination was observed at 12 K. The NBE peaks showed some asymmetry toward the lower energy side, possibly due to compositional fluctuations in the films.
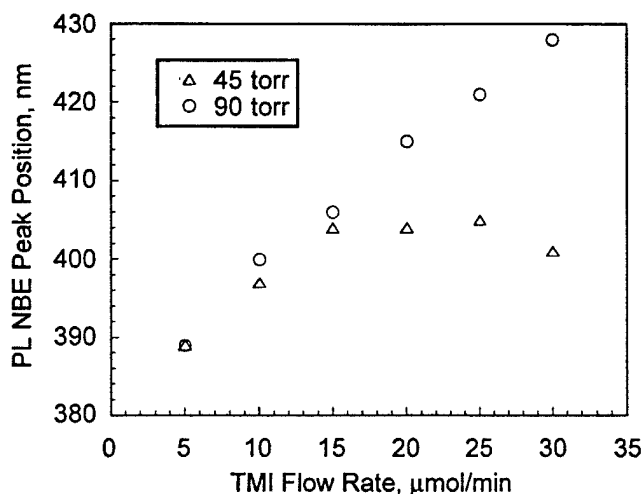

Figure 2.   The dependence of the photoluminescence peak position at 12 K of $In_xGa_{1-x}N$ films on MOVPE growth pressure and TMI flow rate.

20

The room temperature (RT) and 12 K PL spectra for an $In_{0.23}Ga_{0.77}N$ film are shown in Figs. 4 a) and b), respectively. At RT the peak position is at 433.9 nm (2.858 eV) and the FWHM is 174 meV. The deep level "yellow" emission in the film is weak relative to the NBE emission and no DAP recombinations are observed. At 12 K, the peak position shifts to 428.9 nm (2.891 eV) and the FWHM decreases to 103 meV. The broader peak at RT is most likely due to a higher concentration of free carriers. The 33 meV NBE peak shift for the $In_xGa_{1-x}N$ film is less than that of GaN (65.8 meV) over the same temperature range [16].

D. Conclusions

The growth of $In_xGa_{1-x}N$ films with $x \leq$ ~0.23 was achieved on substrates of 6H-SiC(0001)/AlN buffer layer/GaN heterostructures by low pressure MOVPE with V/III ratios as low as 2,420. Indium droplets were not observed. The InN content in these films was a function of the deposition pressure in the system. Room temperature and 12 K PL spectra showed single-feature NBE emission without DAP recombinations. The FWHM of these spectra increased with increasing indium fraction. The FWHM for an $In_{0.23}Ga_{0.77}N$ film at 12 K was 103 meV.

E. Future Work

Future work includes deposition of $In_xGa_{1-x}N$ alloys with higher InN content through an investigation of additional growth parameters, including growth temperature and TEG flow rate. A TEM study of the defect structure in $In_xGa_{1-x}N$ bulk films is currently underway. Single and multiple $In_xGa_{1-x}N$ quantum well structures, as well as $In_xGa_{1-x}N/GaN$ superlattices will be fabricated to investigate their photoluminescence and structural properties. Blue LED structures with $In_xGa_{1-x}N$ active regions will be fabricated, and the electroluminescence properties of the devices will be determined.
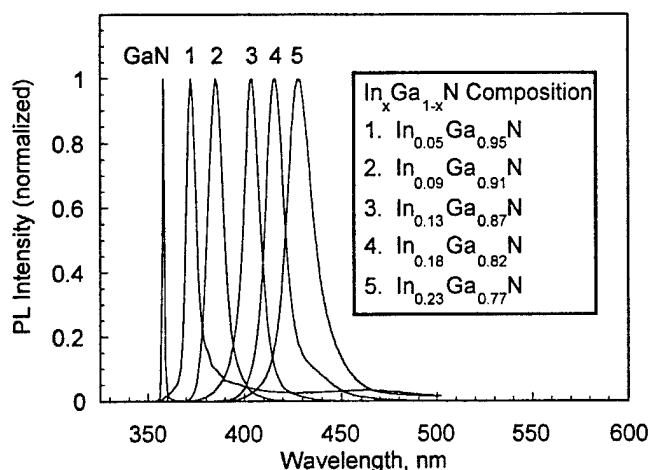
Figure 3.   Photoluminescence at 12 K of GaN and $In_xGa_{1-x}N$ films.
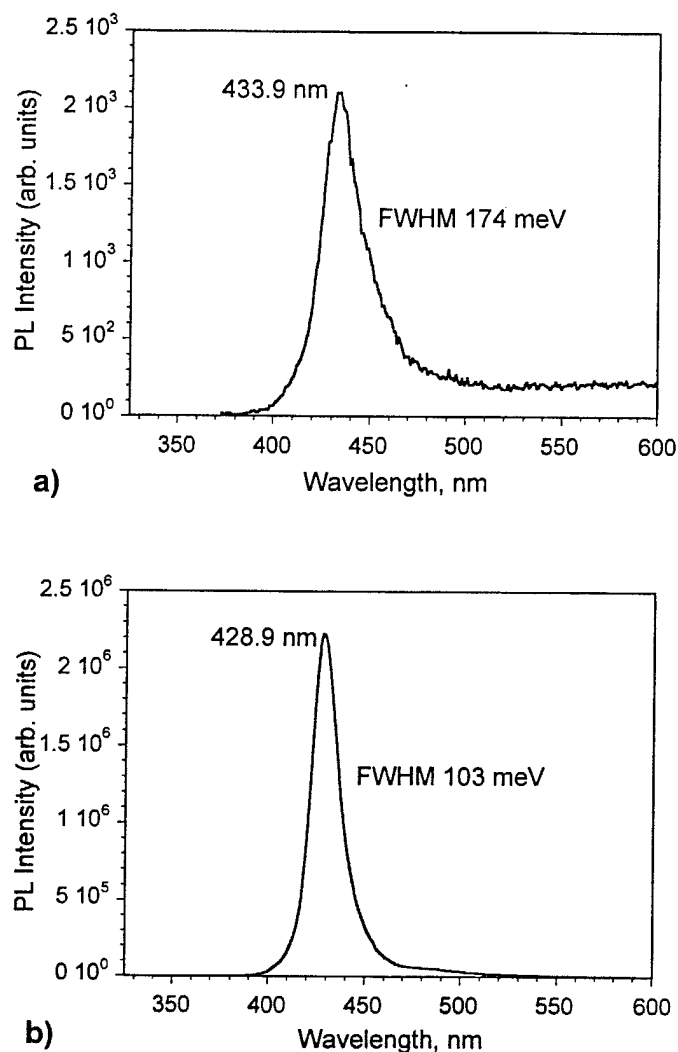
Figure 4.   a) Room temperature and b) 12 K photoluminescence spectra of an $In_{0.23}Ga_{0.77}N$ film. Note the different intensity scales for the two spectra.

F. Acknowledgments

G. References

1. S. Nakamura, M. Senoh, N. Iwasa, S. Nagahama, Jpn. J. Appl. Phys. **34**, L797 (1995).
2. S. Nakamura, J. Cryst. Growth **170**, 11 (1997).
3. R. D. Jones, K. Rose, J. Phys. Chem. Solids **48**, 587 (1987).
4. Q Guo, O. Kato, J. Appl. Phys., **73**, 7969 (1993).
5. I. Ho, G. B. Stringfellow, Appl. Phys. Lett. **69**, 2701 (1996).
6. S. Nakamura, T. Mukai, Jpn. J. Appl. Phys. **31**, L1457 (1992).

7. M. Shimizu, K. Hiramatsu, N. Sawaki, J. Cryst. Growth **145**, 209 (1994).
8. S. Keller, B. P. Keller, D. Kapolnek, U. K. Mishra, S. P. DenBaars, I. K. Shmagin, R. M. Kolbas, S. Krishnakutty, J. Cryst. Growth **170**, 349 (1997).
9. M. V. Weckwerth, K. P Killeen, R. Biefeld, T. Drummond, M. H. Crawford, J. C. Zolper, Electronic Materials Conference, Santa Barbara, June 1996.
10. E. L. Piner, M. K. Behbehani, N. A. El-Masry, F. G. McIntosh, J. C. Roberts. K. C. Boutros, S. M. Bedair, Appl. Phys. Lett. **70**, 461 (1997).
11. N. Yoshimoto, T. Matsuoka, T. Sasaki, A. Katsui, Appl. Phys. Lett. **59**, 2251 (1991).
12. T. Yuzhen, Z. Guoyi, J. Zhijian, D. Xiaozhong, W. Shumin, Solid State Comm. **102**, 405 (1997).
13. A. D. Hanser, C. A. Wolden, W. G. Perry, T. Zheleva, E. P. Carlson, A. D. Banks, R. J. Therrien, R. F. Davis, submitted to J. Electron. Mater.
14. *Properties of Group III Nitrides*, J. H. Edgar, ed., INSPEC, London, (1994).
15. W. Van der Stricht, I. Moerman, P. Demeester, L. Considine, E. J. Thrush, J. A. Crawley, Internet J. Nitride Semicond. Res. **2**, 16 (1997).
16. W. Shan, T. J. Schmidt, X. H. Yang, S. J. Hwang, J. J. Song, B. Goldberg, Appl. Phys. Lett. **66**, 985 (1995).

V. Growth of GaN and $Al_xGa_{1-x}N$ Thin Films via Organometallic Vapor Phase Epitaxy

A. Introduction

The potential for numerous applications of the III-V nitrides in both optoelectronic and microelectronic devices has led to considerable research concerning the growth and development of these materials. Gallium nitride-based MODFETs are of particular interest because of their high electron mobility and carrier density. Growth of these devices on SiC substrates rather than the more commonly used sapphire takes advantage of the greater thermal conductivity of the SiC, which is especially beneficial for high-power devices.

B. Experimental Procedure

Thin films of GaN and $Al_xGa_{1-x}N$ were deposited on an on-axis 6H-SiC(0001) substrate. A MODFET structure was grown by depositing a thin layer of $Al_xGa_{1-x}N$ on a GaN film. The SiC wafer was dipped in a 10% HF solution for 10 minutes to remove the thermally grown oxide layer and was blown dry with N_2. The substrate was then placed on a SiC-coated graphite susceptor and loaded into a cold-wall, vertical, pancake-style, OMVPE reactor. The system was evacuated until a base pressure of less than 3×10^{-5} Torr was reached. An RF power supply was used to inductively heat the continuously rotating susceptor to the AlN deposition temperature of 1100°C in 3 slm of hydrogen diluent. Once the susceptor reached a temperature of 1100°C (as measured with an optical pyrometer), deposition of the AlN buffer layer was initiated by flowing 23.6 μmol/min triethylaluminum (TEA) and 1.5 slm ammonia (NH_3) into the reactor. Hydrogen was used as the carrier gas for the metalorganics. The system pressure during deposition was maintained at 45 Torr. The AlN buffer layer was grown for 30 minutes, which resulted in a thickness of 1200 Å. After terminating the flow of TEA, the susceptor temperature was decreased to 1000°C and GaN growth was initiated by flowing triethylgallium (TEG) into the reactor at a rate of 26.1 μmol/min. The GaN layer was grown for one hour, resulting in a thickness of ~0.9 μm. A thin layer (~400 Å) of $Al_xGa_{1-x}N$ (x = 0.3) was grown on top of the GaN by flowing 17.3 μmol/min and 14.9 μmol/min of TEG and TEA respectively. Growth temperature for the $Al_xGa_{1-x}N$ was 1100°C.

C. Results

Hall-effect measurements were taken at temperatures of 188 K and 298 K. The results of these measurements are shown in Table I. Scanning electron microscopy (SEM) was performed using a JEOL 6400 FE operating at 5 kV. The SEM image of the film's cross section is shown in Fig. 1.

Table I. Hall Measurement Results

	188 K	298 K
Carrier Concentration	1.236×10^{13} cm^{-2}	1.274×10^{13} cm^{-2}
Resistivity	516.2 W•cm	633.6 W•cm
Mobility	978.67 cm^2/V•s	773.47 cm^2/V•s
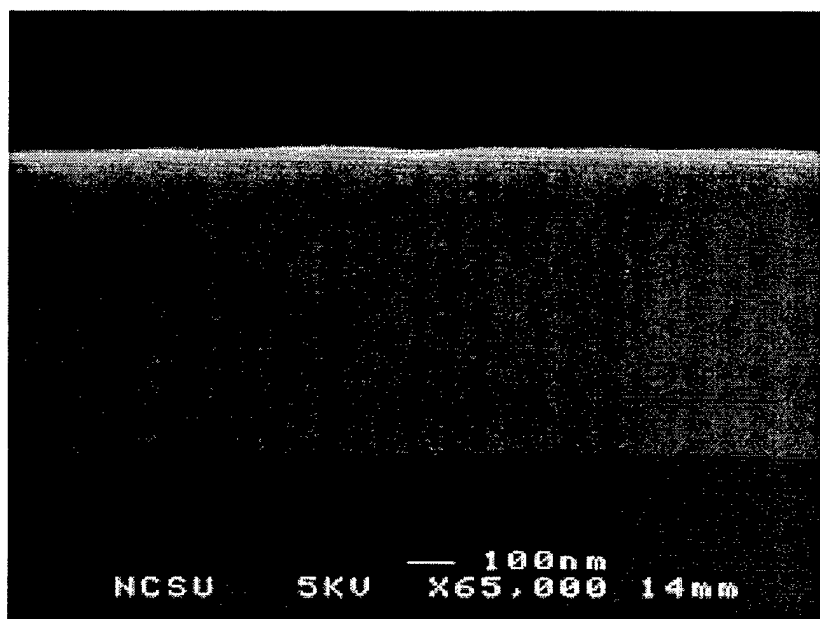
Figure 1.   SEM image of MODFET structure.

D. Conclusions

A MODFET structure of GaN and Al$_x$Ga$_{1-x}$N was grown on on-axis 6H-SiC(0001) at 1000 to 1100°C via OMVPE. Hall measurements were performed to determine the electrical properties of the sample. Scanning electron microscopy was employed to observe the cross section of the film.

E. Future Research

Future research plans include optimizing the Al to Ga ratio in the Al$_x$Ga$_{1-x}$N layer of the MODFET structure. An attempt will be made to grow the top Al$_x$Ga$_{1-x}$N layer such that the Al to Ga ratio will vary from a low to high Al concentration. Other device structures, UV photodetectors in particular, will be investigated. This work will involve experiments in producing *p-i-n* structures with GaN and various alloy compositions of Al$_x$Ga$_{1-x}$N.

VI. Characterization of p-GaN Films Grown by Metalorganic Vapor Phase Epitaxy via Conventional Ni/Au Contacts

A. Introduction

The achievement of p-type conducting GaN has led to the fabrication of such practical devices as blue and green light emitting diodes [1]. Currently, metalorganic vapor phase epitaxy (MOVPE) is the dominant growth technique for the III-V nitrides, and acceptor doping with Mg is the most common method of achieving p-type conduction in GaN. The successful characterization of these p-GaN films is essential to improving film quality and, hence, the overall efficiency of GaN-based devices currently being produced, as well as those being investigated [2].

The following report is a detailed account of the behavior of both the as-deposited and annealed Ni/Au contact schemes used to study the electrical properties of p-type GaN films. The results of Hall measurements made using these contacts are also presented.

B. Experimental Procedure

The 1 micron thick Mg-doped GaN films used in this study were grown via MOVPE on a 1000Å thick AlN buffer layer previously deposited at 1100°C on a 6H-SiC(0001) substrate. For a comprehensive treatment of the growth conditions, see Ref. [3]. Capacitance voltage (C-V) measurements were made on the as-grown films using a Hewlett Packard 4284A C-V measurement system and mercury probe station. Prior to the contact deposition, the GaN was degreased and then followed by a 15-minute dip in either a 1:1 DI:HCl or 100% HCl solution. The samples were immediately loaded into a conventional electron beam evaporator where 500Å Ni and 1000Å Au [4] films were deposited at a base pressure of ~4×10^{-6} Torr. The dot contacts (d=.04 in.) were patterned using a molybdenum shadow mask in contact with the GaN. The contacts were arranged in a square pattern with a contact at each corner and a center to center separation of .1 in. Annealing treatments, which ranged from 400°C–600°C, were performed in N$_2$ ambient using a Heatpulse 410 rapid thermal annealing (RTA) furnace. Hall measurements were made using a Keithley Model 80 Hall System.

C. Results and Discussion

The contacts for those films whose carrier concentrations were 3×10^{17} cm^{-3}, as reported by (C-V) measurements, were rectifying in both the as-deposited and annealed conditions (Fig.1). However, there was considerable improvement in the size of the offset and the overall resistance of the samples when annealed at higher temperatures.

For those films whose carrier concentrations were 5×10^{18} cm^{-3}, the contacts were linear with a slight offset in the as-deposited condition (Fig. 2). These results are consistent with

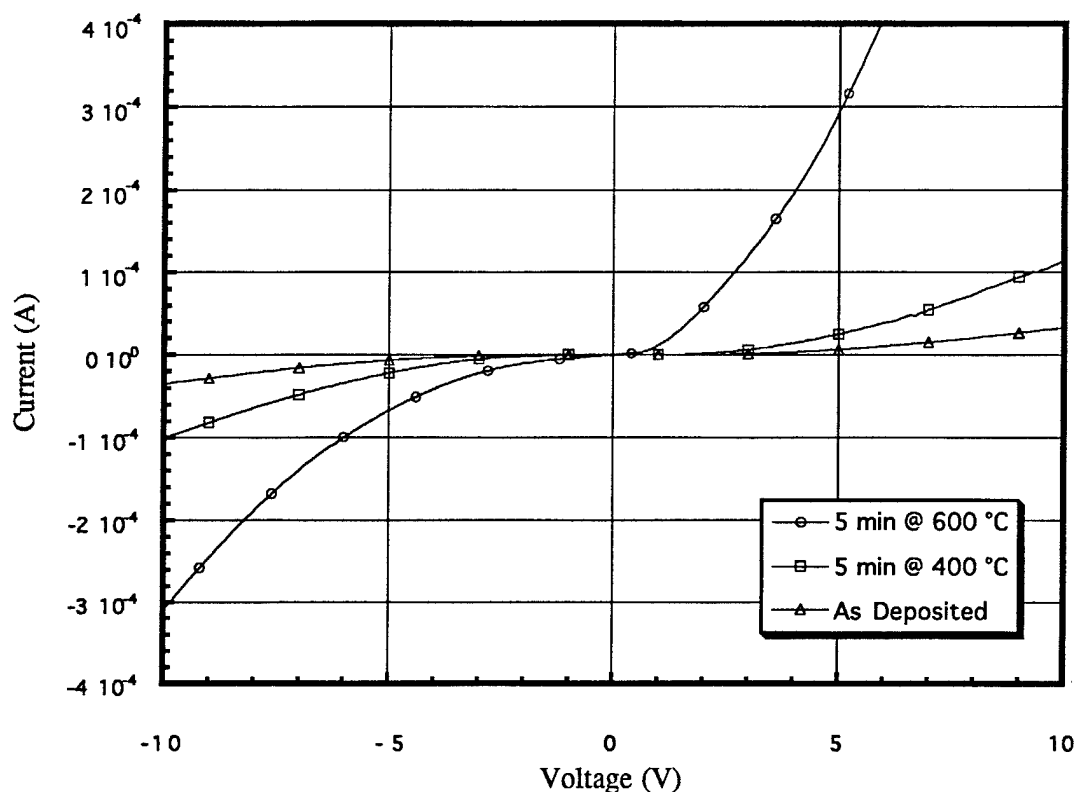Figure 1.   I-V data for Mg-GaN p = 3×10^{17} cm^{-3}.

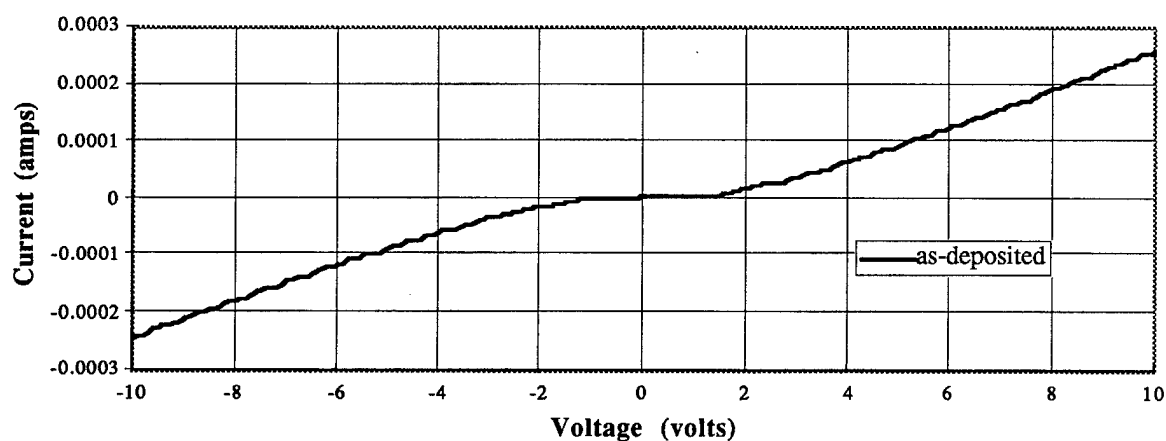

Figure 2.   I-V data for Mg-GaN p = 5×10^{18} cm^{-3} (C-V).

what has been found in earlier experiments [4,5]. However, in an attempt to achieve completely linear behavior, these contacts were annealed at 600°C for 1 minute. Upon annealing, there was complete contact degradation and balling of Au on the Ni surface. These

results contradict earlier findings which showed contact improvement and no degradation of the Au surface when annealed at these temperatures for even longer periods of time (Fig.1). The significant differences in electrical properties amongst these contacts can most certainly be attributed to the difference in carrier concentrations between the films, which in this case was greater than an order of magnitude. This should be expected due to the fact that a film with a higher carrier concentration, which is directly related to the doping level, will have a significantly smaller depletion width upon contact formation. A smaller depletion width increases the probability of tunneling and reduces the barrier to current flow. This reduction in barrier height is evidenced by the small turn-on voltage illustrated in Fig. 2. There may be other factors that are contributing to the differences in behavior between these contacts. However, the large difference in carrier concentration overshadows any of these effects.

Although the contacts illustrated in Fig. 2 have a slight offset (~1 volt), they were linear enough to make Hall measurements which was the ultimate goal of this effort. The Hall measurements resulted in a carrier concentration of 2×10^{17} cm^{-3}, a mobility of ~ 13.45 cm^2 Volt^{-1} sec^{-1} and a film resistivity of 5.6 $\Omega \times$cm.

D. Conclusions

In summary, p-GaN films have been successfully characterized using a Ni/Au contact scheme. Although the contacts were not completely ohmic, the slight offset in the I-V curves did not prevent the use of Hall techniques. It has been shown that the linearity of the contact in the as-deposited condition is dramatically affected by the doping level in the sample. Any attempts to improve the linearity of the contact were unsuccessful due to the fact that the Au balled up on the Ni surface upon annealing. The reason why this behavior is specific to particular samples is unknown at this time.

E. Future Plans and Research Goals

Since these preliminary results indicate that there is a strong relation between contact quality and the doping level in the sample, a more comprehensive investigation is already underway. The Ni/Au scheme described earlier will be deposited on a series of GaN films grown via metalorganic vapor phase epitaxy and doped to different Mg levels. The current voltage characteristics of the contacts in both the as-deposited and annealed conditions, as well as the electrical properties of each film will be studied

Although it is possible to make ohmic contact to p-GaN [4,5], the specific contact resistivities that have been achieved up until the present time are far from device quality. This is no surprise when one considers the fact that GaN, which has a band gap of ≈ 3.4 eV and an electron affinity of χ ≈ 2.7 eV, would require a metal with a work function ≈ 6.1 eV. This certainly presents a problem due to the fact that most metal work functions are never greater

than ≈ 5 eV [6]. Consequently, one is forced into the position of considering a multilevel metallization which would provide an increase in the carrier concentration in the immediate vicinity of the contact or a graded heterostructure in order to achieve a lower specific contact resistivity.

The lowest specific contact resistivity reported to date, which was $\sim 1 \times 10^{-2}$ $\Omega \times cm^2$ [7], has been achieved through the use of a solid phase regrowth (SPR) mechanism. This technique has proven to be very effective in forming low resistance ohmic contacts to p type GaAs [8]. "The regrowth process begins with a low temperature reaction between a metal M (e.g. Ni, Pd, or Pt) and a compound semiconductor substrate AB to produce an intermediate M_xAB or MB_x phase. A subsequent reaction at a higher temperature between an overlayer of Si, Ge, Al or In and the intermediate phase results in the decomposition of the intermediate phase and the epitaxial regrowth of a layer of the compound semiconductor [9]." Another vital feature of this mechanism is that the proper dopant be incorporated during the regrowth. This can be achieved by including the appropriate dopant interlayer placed strategically within the metallization so as to optimize the desired thickness of this highly-doped regrown layer. This SPR mechanism has also been used to make low resistance ohmic contact to n-GaAs where the final product of the Pd/In/Pd/n-GaAs metallization is PdIn/In_xGa_{1-x}As/n-GaAs/ [10]. Although this graded heterostructure has been used for ohmic contact to n-GaAs, no results have been reported regarding it's application to GaN.

It is proposed to utilize this SPR technique to grow a $In_xGa_{1-x}N$ / p-GaN heterostructure so as to grade out the large band gap associated with this material. The metallizations will be as follows: Si/Ni/Mg/In/Ni/p-GaN and Si/Ni/In/Mg/Ni/p-GaN. This metallization was chosen due to the fact that Ni has in some cases been shown to form a NiGaN ternary phase, even at room temperature [7], which is necessary for the first stage of the (SPR) process. At elevated temperatures, it is postulated that a NiSi phase is favored to form which would then lead to decomposition of the intermediate phases and regrowth of GaN with In and Mg incorporation. The most formidable obstacles to be overcome in developing this structure will be selecting the appropriate interlayer thicknesses and annealing treatments so as to achieve both Mg and In incorporation in the regrown InGaN layer. However, the fact that p-type conduction in Mg-InGaN has been observed [11] is quite encouraging.

The as-deposited and annealed metallizations will be characterized electrically, chemically and microstructurally using transmission line model (TLM) measurements, cross bridge Kelvin resistor (CBKR) measurements, secondary ion mass spectroscopy (SIMS), Auger electron spectroscopy (AES), and high resolution transmission electron microscopy (HRTEM). The interlayer thickness, as well as annealing times and temperatures will then be optimized to give the lowest specific contact resistivity.

F. Acknowledgments

G. References

1. S. Nakamura, M. Senoh, N. Iwasa, S. Nagahama, Jpn. J. Appl. Phys. **34**, L797 (1995).
2. Y.-F. Wu, S. Keller, P. Kozodoy, B.P. Keller, P. Parikh, D. Kapolnek, S.P. Denbaars, U.K. Mishra, IEEE Electron. Dev. Lett. **18**, 290 (1997).
3. A. Hanser, C. Wolden, W. Perry, T. Zheleva, E. Carlson, P. Hartlieb, R. F. Davis (same report).
4. J.T. Trexler, S.J. Miller, P.H. Holloway, M.A. Kahn, *Mat. Res. Soc. Symp. Proc.* 395, Pittsburgh, PA (1996), pp. 819-824.
5. T. Kim, Myung C. Yoo, and T. Kim, *Mat. Res. Soc. Symp. Proc.* 449, Pittsburgh, PA (1997), pp. 1061-1065.
6. D.R. Lide, *Handbook of Chemistry and Physics*, Chemical Rubber, Boston, 1991.
7. E. Kaminska, A. Pitrowska, A. Barcz, L. Ilka, M. Guziewicz, S. Kasjaniuk, E. Dynowska, S. Kwiatkowski, M.D. Bremser, R.F. Davis (unpublished).
8. C.C. Han, X.Z. Wang, L.C. Wang, E.D. Marshall, S.S. Lau, S.A. Schwarz, C.J. Palmstrom, J.P. Harbsison, L.T. Florez, R.M. Potemski, M.A. Tischler, T.F. Kuech, J. Appl. Phys. **68**, 5714 (1990).
9. T. Sands, E.D. Marshall, and L.C. Wang, J. Mater. Res. **3**, 914 (1988).
10. D.Y. Chen, Y.A. Chang, D. Swenson, J. Appl. Phys. **81**, 297 (1997).
11. S. Yamasaki, S. Asami, N. Shibata, M. Koike, K. Manabe, T. Tanaka, H.Amano, I. Akasaki, Appl. Phys. Lett . **66** (9), 27 (1995).

VII. High Rate and Selective Etching of GaN, AlGaN, and AlN Using an Inductively Coupled Plasma

S. A. Smith[a], C. A. Wolden, M. D. Bremser, A. D. Hanser, and R. F. Davis
Department of Materials Science and Engineering, North Carolina State University, Raleigh, North Carolina 27695-7919

[a] Permanent address: Materials Directorate, Air Force Research Laboratory, Wright Patterson Air Force Base, OH 45433-7750

W. V. Lampert
Materials Directorate, Air Force Research Laboratory, Wright Patterson Air Force Base, OH 45433-7750

The etching behavior of gallium nitride (GaN), aluminum gallium nitride ($Al_xGa_{1-x}N$), and aluminum nitride (AlN) has been systematically examined in an inductively coupled plasma (ICP) using Cl_2 and Ar as the reagents. Etch rates were strongly influenced by ICP power and DC bias, while relatively insensitive to pressure, flow rate, and gas composition. Maximum etch rates of 9,800 Å/min for GaN, 9,060 Å/min for $Al_{.28}Ga_{.72}N$, and 7,490 Å/min for AlN were attained. The etch profiles were highly anisotropic over the range of conditions studied. The DC bias had to exceed certain voltages before significant etch rates were obtained. These values were <-20 V for GaN, -40 V for $Al_{.28}Ga_{.72}N$, and >-50 V for AlN. As such, increasing selectivity for GaN over $Al_{.28}Ga_{.72}N$ and AlN was achieved at DC biases below -40 V. At -20 V, the GaN etch rates were 38 times greater than AlN and a factor of 10 greater than $Al_{.28}Ga_{.72}N$. These results demonstrate the importance of ion bombardment in the etching of these materials.

The realized and future potential of GaN, AlN, and $Al_xGa_{1-x}N$ for short wavelength light emitters and detectors, and high-temperature and high-power electronics is considerable.[1,2] Etching anisotropic features is a crucial step in the fabrication of many of these devices. Wet chemical etching of GaN has to date produced only slow etch rates and isotropic etch profiles,[3] both of which are undesirable for commercial applications. Dry etching is an attractive alternative from which one can achieve controlled degrees of anisotropy, high etch rates, material selectivity, low damage, and the ability to control an etch stop

The four primary dry techniques that have been employed to etch GaN are reactive ion etching (RIE), electron cyclotron resonance etching (ECR), magnetron reactive ion etching (MIE), and inductively coupled plasma etching (ICP).[4-6] The slowest etch rates and the lowest degree of anisotropy were determined for RIE. This has been attributed to the low plasma densities and the higher operating pressures inherent in this technique. The other three process routes are high density, low pressure alternatives to the parallel plate reactor. To date, the use of ECR has produced the fastest GaN etch rates of 13,000 Å/min with an ICl chemistry.[7] Rates of 6,875 Å/min were attained with an ICP system and a $Cl_2/H_2/Ar$ mixture.[8]

Chlorine-based gases such as BCl_3, $SiCl_4$, and Cl_2 are the primary reagents that have been employed to etch the III-Nitrides. Vartuli et al. have reported a dry technique that etches GaN selectively with respect to AlN and $Al_xGa_{1-x}N$.[9,10] Selectivities of 10 between GaN and AlN, and 4 between GaN and $Al_{.31}Ga_{.69}N$ were reported. In this letter we report the results of a systematic study of ICP etching of III-Nitrides using a Cl_2/Ar chemistry. Selective etching of GaN relative to both AlN and $Al_{.28}Ga_{.72}N$ was achieved by controlling the DC bias. The dependence of the etch rate on both ICP power and DC bias are also reported for the three materials. Lastly, the anisotropic nature of the etch profiles is demonstrated.

The ICP system was a custom built, 41 cm diameter by 58 cm tall, loadlocked stainless steel chamber. The RF power was coupled through a 32.4 cm diameter quartz window at the top of the chamber. The inductive source was a planar, 4 turn, 23 cm diameter copper coil which was connected to a RF Power Products 2 kW RF generator operating at 13.56 MHz via an autotuning matching network. Gas was fed into the chamber through a stainless steel shower ring positioned level with the bottom of the quartz window. A water-cooled wafer chuck was mounted on a motor driven vertical translation stage which had 30.5 cm of travel. This allowed samples to be transferred between the loadlock chamber and the processing zone. A second 500 W RF source was connected to the wafer chuck to apply a controllable DC bias to the substrate. The substrate cooling water was maintained at 16°C to prevent the baking of photoresist during etching. The chamber was evacuated by an Alcatel 900 l/s turbomolecular pump which attained a base pressure of 10^{-7} Torr.

A magnetic bucket containing 240 Nd-Fe-B magnets was mounted on the outside perimeter of the chamber to increase the plasma density by confining the electrons to a central volume

within the chamber. This reduced electron losses due to collisions with the chamber walls. The ions were also confined due to electrostatic coupling with the electrons. The former were not directly affected by the magnetic field.[11]

The GaN, AlN, and Al$_{.28}$Ga$_{.72}$N samples used for this study were epitaxially grown on 6H-SiC-(0001) substrates via metalorganic vapor phase epitaxy (MOVPE) using trimethyl-aluminum (TMA) and triethylgallium (TEG) as the Al and Ga sources, respectively, and NH$_3$ as the nitrogen source.[12,13] An ≈100nm AlN buffer layer was deposited on the SiC substrates prior to the growth of the GaN and the Al$_{.28}$Ga$_{.72}$N. Preparation of the samples for etching employed the sequence of applying a Ni coating, patterning with photoresist, and dipping into HNO$_3$ to etch away the Ni and into acetone to remove the photoresist. Just prior to entry into the etching system, the samples were dipped into 10% HF acid for 10 minutes to remove oxygen and carbon contaminants. Samples were attached to a 7.6 cm diameter anodized aluminum transport plate using vacuum grease which was mounted onto the wafer chuck. After entry into the system a base pressure of ≤5×10^{-7} Torr was attained before the etching experiments were initiated.

The etch rates were determined by the step heights measured using a Dektak II profilometer. Anisotropy was determined by scanning electron microscopy (SEM). Other effects such as electrical damage, physical damage, and chemical contamination are currently being investigated.

The etching parameters studied and the ranges examined are summarized in Table I. The DC bias was varied instead of bias power since the former more directly determines the energy of the ions which strike the surface. The three samples were etched simultaneously to ensure accurate comparisons. It was determined that the gas phase concentration and total flow rate within the ranges shown in Table I had no significant impact on the etch rates (<20%). The etch rate was slightly more sensitive to pressure, varying 44% over the range investigated. A more extensive study of all parameters using optical emission spectrometry (OES) and mass spectrometry will be reported at a later date.

Table I. The Experimental Parameters Examined, Their Ranges,
and the Base Conditions Employed in This Study

Parameter	Range	Base Cond.
ICP Power	100-1100 W	500 W
DC Bias	20-450 (-V)	-150 V
Pressure	1-9 mTorr	5 mTorr
Total Flow Rate	10-30 sccm	25 sccm
Cl$_2$ Percentage	50-100%	80%
Ar Percentage	0-50%	20%

Figure 1 shows that the etch rates for the three materials as a function of ICP power for the three materials behaved similarly. The etch rates increased rapidly from 100 to 500W. Above 500 W the rate of increase was slightly attenuated, although no maximum was reached. Between 900 and 1100 W, the etch rates of the $Al_{.28}Ga_{.72}N$ closely matched those of the GaN. The observed increase in the etch rates with ICP power was likely due to increases in both the reactive chlorine concentration and the ion density. Additional diagnostics are necessary to distinguish between these two effects. The maximum etch rates achieved at an ICP power of 1100 W were 9,140 Å/min for the GaN, 9,060 Å/min for the $Al_{.28}Ga_{.72}N$, and 7,490 Å/min for the AlN.

The etch profiles were highly anisotropic over all conditions examined. Figure 2 shows a typical profile obtained under the base conditions (see Table I) using nickel as the etch mask. The vertical striations were transferred from imperfections in the mask edge. The etched surface was smooth and appeared to be free of physical damage such as pitting.

The DC bias had a very pronounced effect on the etch rates for all three materials, as shown in Figure 3. Again, the behavior was qualitatively similar for the three materials. Firstly, each material had a threshold voltage below which the etch rates were very low. These voltages were: <-20 V for GaN, ~-40 V for $Al_{.28}Ga_{.72}N$, and between -50 and -150 V for AlN. Above the threshold value the rates increased dramatically to -250 V at which point a plateau occurred for the three materials. Between -350 and -450 V the rates increased again, suggesting that an additional etching mechanism may be operative at these high biases. The maximum rates achieved at a DC bias of -450 V were 9,800 Å/min for GaN, 8,670 Å/min for $Al_{.28}Ga_{.72}N$, and 6,700 Å/min for AlN.
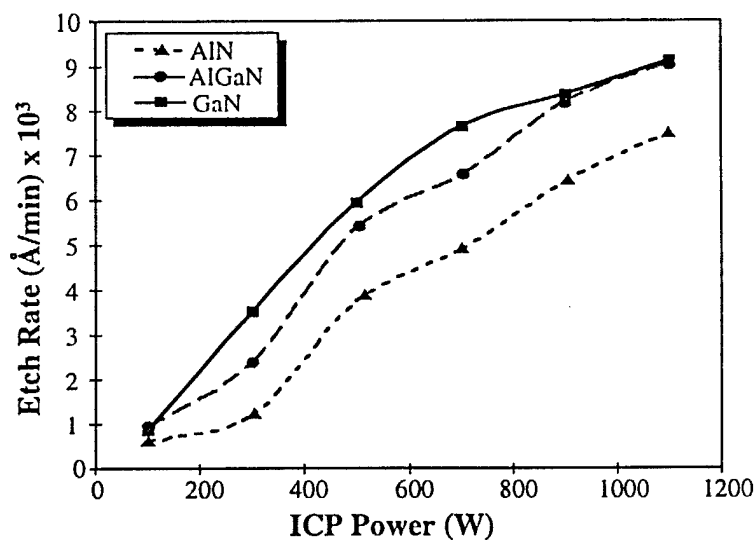

Figure 1.   The etch rates of GaN, $Al_{.28}Ga_{.72}N$, and AlN as a function of ICP power.
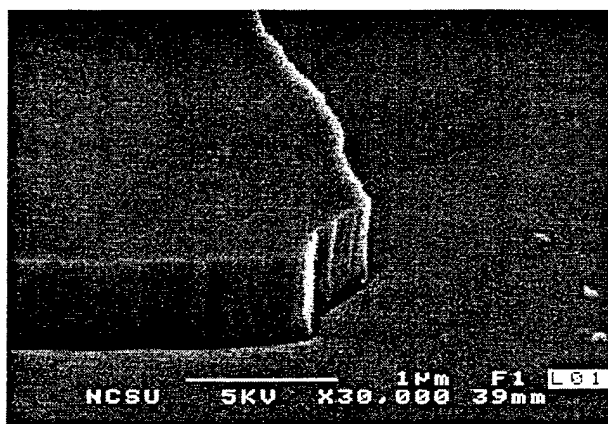
Figure 2.   Typical etch profile using Ni as the etch mask under base conditions. Vertical striations were transferred from imperfections in the mask edge.
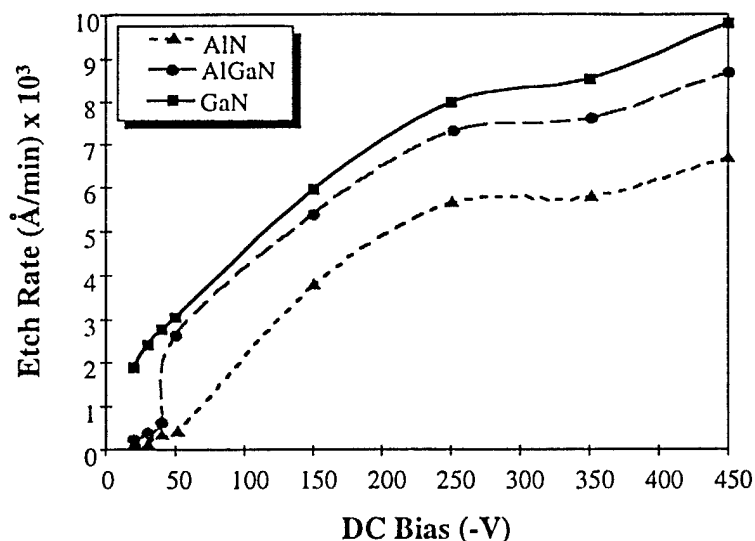

Figure 3.   The etch rates of GaN, $Al_{.28}Ga_{.72}N$, and AlN as a function of DC bias.

The etch selectivity of GaN relative to AlN and $Al_xGa_{1-x}N$ is of significant interest for the fabrication of $Al_xGa_{1-x}N$ based heterostructure devices. One example is the etch penetration through a GaN capping layer to the $Al_xGa_{1-x}N$ recessed gate in a high electron mobility transistor. Etching of the latter material should be minimal. Selective etching was achieved at low DC biases. The data from Figure 3 was converted into selectivity and plotted in Figure 4 for GaN relative to $Al_{.28}Ga_{.72}N$ and AlN over the range of -(20-50 V). The selectivity is the ratio of the etch rate of GaN to the AlN or $Al_xGa_{1-x}N$. At -50 V, the selectivity between GaN and AlN was 8.5; whereas, it was only 1.2 between the GaN and $Al_{.28}Ga_{.72}N$. The greatest selectivities for GaN were found at a bias of -20 V, a factor of 38 over AlN and approximately 10 over $Al_{.28}Ga_{.72}N$. These differences in etch rates are consistent with the different bond energies between Ga-N and Al-N of 8.92 eV/atom and 11.52 eV/atom, respectfully.[14] A

35

second factor is the lower volatility of $AlCl_x$ relative to $GaCl_x$. Since lower DC biases were used to attain the selective etching, there is a tradeoff between the selectivity and the total etch rate.

The strong dependence of the etch rate on DC bias indicates that ion bombardment plays a significant role in the etching of these materials. Ion bombardment can enhance etching via damaging the surface to make it more reactive, stimulating desorption of the etch products, and direct physical sputtering. The existence of a threshold bias indicates that breaking Ga-N or Al-N bonds by ion bombardment may be the rate-limiting step. It is presumed that ion damage increases the reactivity of these ordinarily inert materials. The ion-induced damage may be necessary to form the volatile $GaCl_x/AlCl_x$ etch products.

In summary, dry etching of GaN, AlN, and $Al_{.28}Ga_{.72}N$ have been investigated in an ICP system using Cl_2 and Ar as the process gases. The rates for all three materials depended strongly on both the ICP power and the DC bias. Maximum etch rates of 9,800 Å/min for the GaN, 9,060 Å/min for the $Al_{.28}Ga_{.72}N$, and 7,490 Å/min for the AlN were achieved which are the highest reported to date for this chemistry. Threshold biases of >-50V and -40V were required to induce significant etching for AlN and $Al_{.28}Ga_{.72}N$. No threshold was found for GaN down to -20 V. As a result, selectivities of 38 between GaN and AlN and 10 between GaN and $Al_{.28}Ga_{.72}N$ were obtained at a DC bias of -20V. This is of potential interest for the fabrication of $Al_xGa_{1-x}N$ based heterostructure devices. Research is ongoing to quantify the effects of plasma induced damage and to better understand the underlying mechanisms.

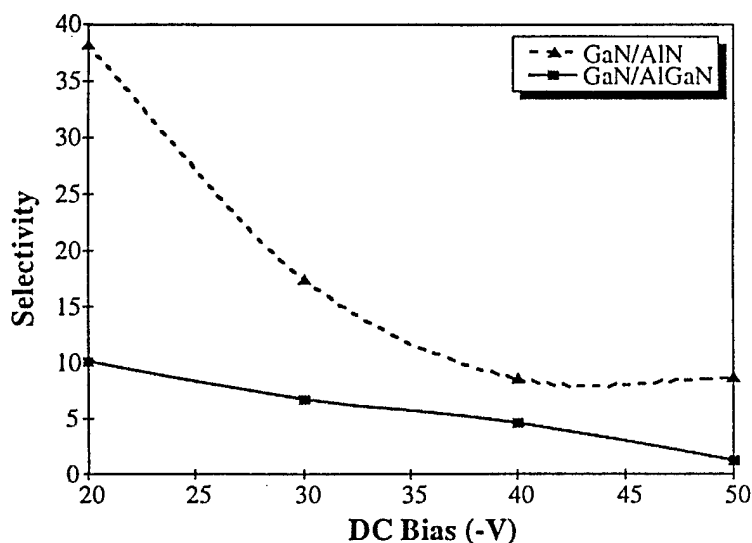Figure 4. The selectivity of GaN relative to $Al_{.28}Ga_{.72}N$ and AlN as a function of DC bias. Values of selectivity were obtained from the GaN/AlN and GaN/$Al_{.28}Ga_{.72}N$ etch rate ratios using the data for the individual etch rates shown in Figure 3.

References

1. R.F. Davis, Proc. IEEE **79**, 702 (1991).
2. H. Morkoç, G.B. Gao, M.E. Lin, B. Suerdlov, and M. Burns, J. Appl. Phys. **76**, 1363 (1994).
3. S. J. Pearton, C. R. Abernathy, F. Ren, J. R. Lothian, P. W. Wisk, and A. Katz, J. Vac. Sci. Technol. A **11** (4), 1772 (1993).
4. R. J. Shul, S. P. Kilcoyne, M. Hagerott Crawford, J. E. Parmeter, C. B. Vartuli, C. R. Abernathy, and S. J. Pearton, Appl. Phys. Lett. **66** (14), 1761 (1995).
5. M. E. Lin, Z. F. Fan, Z. Ma, L. H. Allen, and H. Morkoç, Appl. Phys. Lett. **64** (7), 887 (1994).
6. G. F. McLane, T. Monahan, D. W. Eckart, S. J. Pearton, and C. R. Abernathy, J. Vac. Sci. Technol. A **14** (3), 1046 (1996).
7. C. B. Vartuli, S. J. Pearton, J. W. Lee, J. Hong, T. D. Mackenzie, C. R. Abernathy, and R. J. Shul, Appl. Phys. Lett. **69** (10), 1426 (1996).
8. R. J. Shul, G. B. McClellan, S. A. Casalnuovo, D. J. Rieger, S. J. Pearton, C. Constatine, C. Barratt, R. F. Karlicek Jr., C. Tran, and M. Schurman, Appl. Phys. Lett. **69** (8), 1119 (1996).
9 C. B. Vartuli, S. J. Pearton, J. W. Lee, A. Y. Polyakov, M. Shin, D. W. Greve, M. Skronowski, and R. J. Shul, Electrochem. Soc. **144** (6), 2146 (1997).
10. C. B. Vartuli, S. J. Pearton, J. D. Mackenzie, C. R. Abernathy, and R. J. Shul, Electrochem. Soc. **143** (10), L246 (1996).
11. E. R. Lory, Solid State Technology (Nov.), 117 (1984).
12. A. D. Hanser, C. A. Wolden, W. G. Perry, R. Therrien, and R. F. Davis, submitted to Journal of Electronic Materials .
13. M. D. Bremser, W. G. Perry, T. Zheleva, N. V. Edwards, O. H. Nam, N. Parikh, D. E. Aspnes, and R. F. Davis, MRS Internet J. Nitride Semicond. Res. **1**, 8 (1996).
14. R. J. Shul, R. D. Briggs, S. J. Pearton, C. B. Vartuli, C. R. Abernathy, J. W. Lee, C. Constantine, and C. Barratt, Mater. Res. Soc. Symp. Proc. **449**, 969 (1996).

VIII. Boron Nitride for Cold Cathode Applications

A. Introduction

Cubic boron nitride (c-BN) thin films have been investigated extensively for their potential in tribological and electronic applications. Possessing a hardness second only to that of diamond, c-BN thin films are stable over an extremely large temperature range and are chemically inert to oxygen and ferrous materials, thus c-BN displays equal promise as an electronic material. A III-V wide band gap (6.4 eV) material, c-BN has been shown to have effective p- and n-type dopants: Be and Si, respectively [1]. Of even greater interest, however, is that intrinsic c-BN has been shown to exhibit a negative electron affinity (NEA) [2]. The smooth surface of c-BN films provides a distinct advantage over CVD-diamond. For these reasons, n-type c-BN has been highly regarded as a potential flat film field emitter.

This section reports on attempts to utilize these qualities to produce c-BN thin films which act as efficient electron emitters. Furthermore, the potential of h-BN, also a wide band gap material, was considered as a field emitter.

B. Growth of c-BN and h-BN

Aside from high-temperature, high-pressure methods, the synthesis of phase pure c-BN has remained somewhat of an enigma. BN thin films containing varying amounts of cubic phase have been synthesized via numerous techniques; each displays evidence of the same progression from random film to a hexagonal phase, but only via energetic means (i.e. ion bombardment) has the nucleation of a cubic phase been observed. Ion beam assisted deposition (IBAD), a common technique with proven success in c-BN synthesis [3], was employed in these studies. A Hanks HM^2 e-gun was used to evaporate boron from a 10cc crucible. The depositing B atoms were concurrently bombarded with N_2^+ and Ar^+ ions from a Kauffman-type ion source. The growth mechanism of BN is not well understood, and there have been several models proposed for the nucleation of c-BN. There seems to be agreement, however, that the mechanism is a strong function of ion flux to boron atom arrival ratio, ion energy and substrate temperature. The growth "window" in parameter space is rather small, and calibrating instruments to operate within this window can prove difficult.

After the work of D. Kester [3], several modifications were made to the IBAD chamber which, when our work began, required retrofitting. In addition, a lack of thorough documentation increased the difficulty of regaining past results. Each time a piece of equipment required maintenance, the system had to be recalibrated, negating any progress which had been achieved. Following an extended period of trial and error, success was finally obtained in locating the parameter space where c-BN could be synthesized. In order to identify the most efficient combination of deposition parameters, those with the greatest sensitivity (ion beam

energy and ion beam current) were varied independently and sequentially. Some results of these studies can be seen in Fig. 1 and Fig. 2. By comparison, this data is in good agreement with the results of Kester [3] and Reinke [4], revealing the same boundaries for h-BN and c-BN nucleation. Above 700 eV, no film was deposited. With an ion/atom arrival ratio of about 2, this value exceeds the repsutter limit. Below 400 eV, only h-BN was deposited, indicating that the ion/atom arrival ratio had fallen beneath the threshold for c-BN nucleation.

Preliminary compositional evaluation of BN films was carried out via FT-IR spectroscopy. A vibrational spectroscopy, FT-IR is sensitive to the bonding state in the films. Therefore, in transmission mode, the percentages of sp^2 and sp^3 bonding can be estimated. In good agreement with the literature, the highest percentage c-BN achieved in the films by IBAD was 85-90%. While conclusive identification may not be achieved without complementary measurements [5], the FT-IR measurements were a time efficient means of evaluating the experimental results. The ease of FT-IR measurements motivated the use of infrared-transparent Si as a substrate.

Major improvements have been achieved in the adhesion of c-BN films during the past 4 months. In the past, delamination of films containing even small percentages of c-BN was observed after only two or three days. Due to a new cleaning procedure prior to deposition, very good adhesion for thin c-BN films (< 2000 Å) was observed. Even c-BN films with
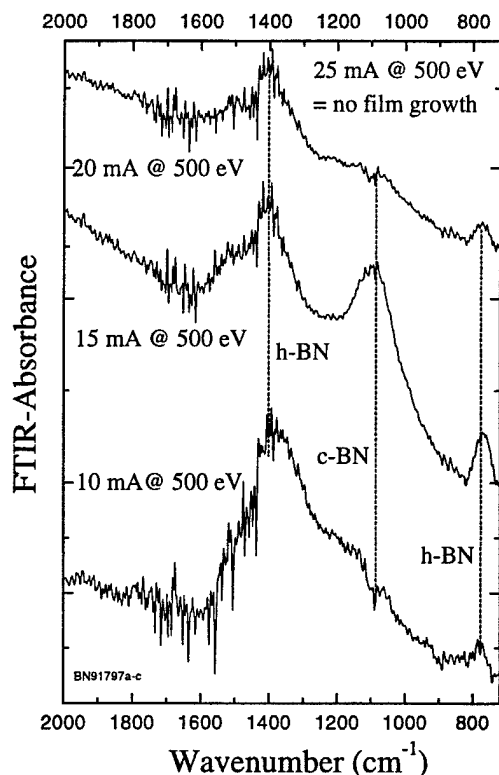

Figure 1.   FTIR-absorbance spectra of BN films deposited with different ion current densities. c-BN growth was achieved with 15 mA.

39

very high phase content (85-90%) have not delaminated after 2-3 months. The substrates were cleaned with acetone before transfer into the IBAD system; then sputter-cleaned with 1 keV Ar$^+$ ions immediately prior to film deposition.

C. Doping with Si During Film Growth

As a means of introducing Si into the film, a mixture of Silane (SiH$_4$) 10 ppm in nitrogen was prepared and brought to the surface of the substrate during film deposition (Fig. 3). Thermal decomposition of the silane would be expected, as the substrate temperature is between 400–500°C. The concentration of the silicon source was low for safety reasons: it was the authors' intention to use preliminary evidence of Si incorporation at low levels to justify the purchase and construction of equipment which would allow storage and flow of higher concentrations of SiH$_4$. The flow of the gas mixture into the IBAD chamber was controlled by an MKS mass flow controller. In the experiments, the BN growth parameters remained constant (the optimal set as determined above), and the flow rate of the gas mixture was varied from 0–7 sccm. Above 7 sccm the pressure in the chamber exceeded 5×10^{-4} Torr, causing the ion source discharge to become unstable. A definitive decrease in c-BN content was observed with increasing flow rate of the silane mixture (Fig. 4). This decrease could be due
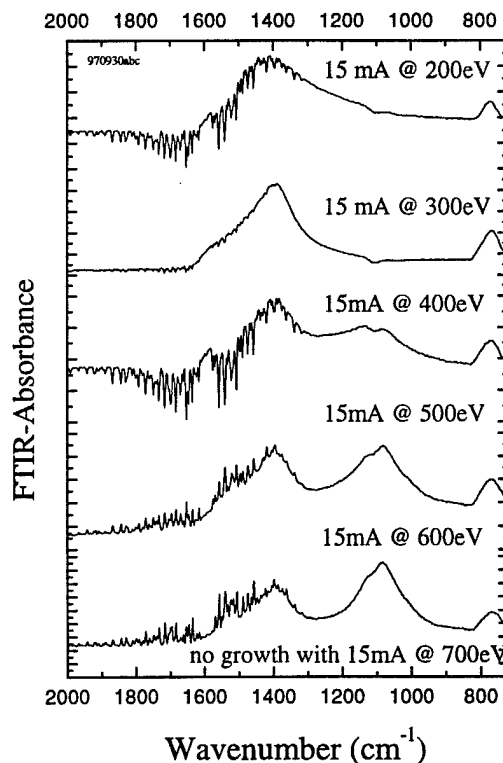

Figure 2.   FTIR-absorbance spectra of BN films deposited with different ion energies. c-BN growth was achieved between 400 and 600 eV.

40

to increased collisions of ions with the gas resulting in a lower ion/atom arrival ratio at the substrate surface, a lower surface temperature of the substrate, or possibly the incorporation of Si atoms. Investigation is ongoing to identify the source of this effect. *In situ* XPS measurements reveal no Si peak in their spectra, so Si concentration is less than .1 atomic percent. Secondary ion mass spectroscopy (SIMS) measurements of the films are under preparation in order to determine Si incorporation in the film.

As an alternate method of Si introduction, simultaneous electron beam evaporation of Si will be investigated. This method of doping will undoubtedly prove challenging, as limiting the amount of Si evaporation to doping levels could be difficult. In addition, there might be enough cross-contamination of boron at the quartz crystal rate monitor to cause erroneous thickness readings. However, B-Si-N alloys may prove to be of interest.

D. Field Emission and FEED

I-V field emission curves were taken under UHV conditions for one undoped c-BN sample grown on n-type Si. These measurements indicate a threshold field of about 75 V/μm for a current of 10 nA. This value is well below of that of uncoated Si. Experiments with the Si-doped c-BN samples are under preparation, however, field emission electron distribution measurements were performed on undoped and doped BN samples. This technique is described elsewhere [6].
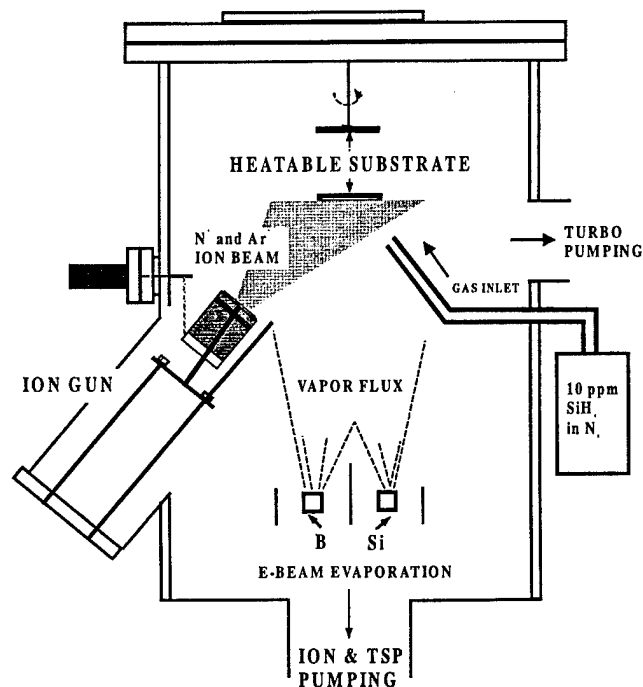

Figure 3.   IBAD-system for the growth of Si-doped BN-films. Si can be incorporated by to ways: (i) SiH$_4$-flow over the sample surface or (ii) by e-beam evaporation.
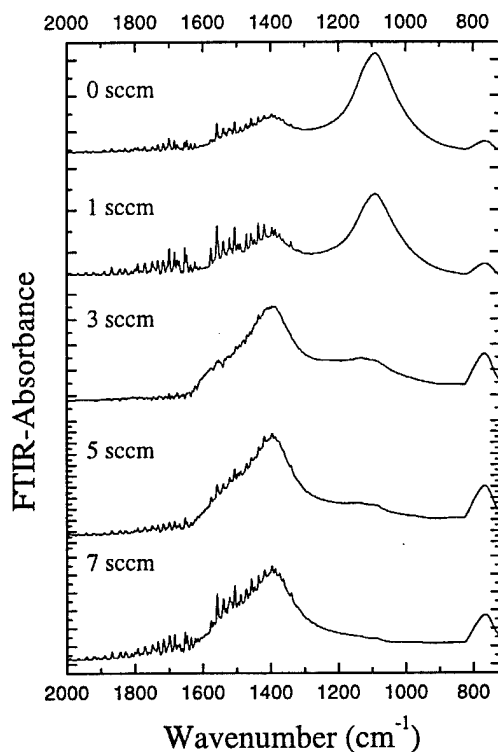
Figure 4.   FTIR-absorbance spectra of BN prepared under different SiH₄ flow.

Figure 5 shows that the energy (E-E$_F$) of the electrons emitted from the c-BN coated Si decreased linearly with applied voltage. Extrapolation of the peak position data to flat-band condition (0 V) yields an intercept of 1 eV. This indicates the field-emitted electrons originated slightly above the Fermi level of the film. Photoelectron measurements showed a vacuum level of about 5 eV above the Fermi level of the film. Therefore, it is most probable that the Fermi level is midgap, and electron transport through the film is due to hopping conduction at localized states in a band at the Fermi level. This suggestion is supported by the fact that the energy distribution of the field emitted electrons increases with increasing voltage (Fig. 5) and by Ref. [7]. The high amount of localized states in the c-BN material is due to the high density of grain boundaries and defects of the nano-sized polycrystalline film. For both undoped and doped c-BN and h-BN samples, similar spectra were measured, indicating that doping in this way does not shift the fermi level in c-BN. However, the incorporation of Si by this method is still questionable (see above). Summarizing, smooth field emitting BN films on silicon substrates were produced.

E. Future Work

Interesting data have been collected thus far, and a more complete understanding of the implications must be reached in order to formulate an interpretation. Experiments to resolve the origin of the decrease in c-BN content with increasing gas flow will be undertaken. By
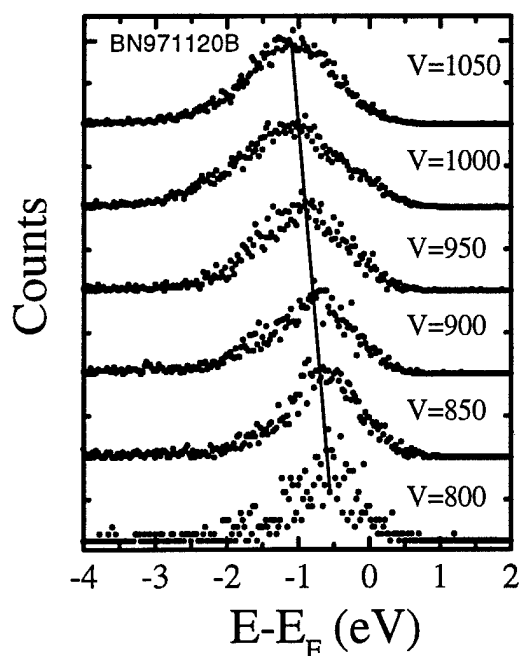
Figure 5.   FEED spectra of a h-BN film deposited on Si. Data were recorded at several different applied voltages.

increasing the ion current and temperature (independently) for a given flow rate, the possibility of synthesizing films with higher c-BN content will be explored. In additon, SIMS data will provide a more complete picture of the phenomenon. More FEED spectra and I-V measurements for BN films on different substrates will be taken to clarify the field emission characteristics of our films.

F. References

1.   O. Mishima *et al.* Science **238** (1987) 181, APL **53** (1988) 962.
2.   M.J. Powers *et al.* APL **67** (1995) 3912.
3.   D.J. Kester *et al.* J. Mat. Res. **8** (1993) 1213.
4.   S. Reinke *et al.* Dia. Rel. Mat. **4** (1995) 272.
5.   P.B. Mirikarimi *et al. to be published in* Mat. Sci. Eng. Rep.
6.   B.L. McCarson *et al. to be published in* APL.
7.   C. Ronning *et al.* Dia Rel. Mat. (1997) 1129.

IX. Distribution List

Dr. Colin Wood   3
Office of Naval Research
Electronics Division, Code: 312
Ballston Tower One
800 N. Quincy Street
Arlington, VA 22217-5660

Administrative Contracting Officer   1
Office of Naval Research
Atlanta Regional Office
100 Alabama Street, Suite 4R15
Atlanta, GA 30303

Director, Naval Research Laboratory   1
ATTN: Code 2627
Washington, DC 20375

Defense Technical Information Center   2
8725 John J. Kingman Road, Suite 0944
Ft. Belvoir, VA 22060-6218